Paleostress Evolution of the Northern Andes as a Key to Plate Kinematics Evolution of the Caribbean Region (Eastern Cordillera of Colombia)

M. Cortés, J. Angelier, B. Colletta

Paleostress evolution of the northern Andes (Eastern Cordillera of Colombia): Implications on plate kinematics of the South Caribbean region

Martín Cortés[1] and Jacques Angelier

Laboratoire de Tectonique, Université Pierre et Marie Curie, Paris, France

Bernard Colletta

Institut Français du Pétrole, Rueil-Malmaison, France

Received 6 June 2003; revised 7 July 2004; accepted 16 September 2004; published 9 February 2005.

[1] New tectonic field data and paleostress determinations in the Eastern Cordillera of Colombia enable us to identify stress regimes that prevailed in the northern Andes since Late Cretaceous times until present day. These regimes were characterized by an E-W to WSW-ENE active contraction from Late Cretaceous to late Paleocene. This direction subsequently changed to NW-SE and finally became WNW-ESE during the Andean tectonic phase. The characteristics and relative chronology of these regimes were deduced from field structures and stratigraphic criteria, using stress inversion of fault slip data sets. To evaluate our model, we used the rotation poles of the South America, Caribbean and Nazca plates relative to North America, and paleogeographic reconstructions of the Caribbean region to derive a kinematic model of the northern Andes. Assuming a general correspondence between the regional convergence directions and the regional compression, we built a theoretical model of the regional stress regimes based on kinematics of the northwestern South America since Late Cretaceous times. This model reveals a major variation at the end of the Paleocene when relative divergence shifted to convergence between the Americas. This is in agreement with our tectonic model based on independent tectonic field data inversion in the Eastern Cordillera. This regional kinematic and tectonic change, which affected the Caribbean at the end of the Paleocene, was responsible for, and consistent with, the major change in stress patterns and structural style in the Eastern Cordillera. It is also coeval with the development of a major regional unconformity in Colombia. **Citation:** Cortés, M., J. Angelier, and B. Colletta (2005), Paleostress evolution of the northern Andes (Eastern Cordillera of Colombia): Implications on plate kinematics of the South Caribbean region, *Tectonics*, *24*, TC1008, doi:10.1029/2003TC001551.

1. Introduction

[2] The northern Andes mountain belt in Colombia is a complex tectonic region close to the triple junction of the continental plate of South America with the Caribbean and the Nazca oceanic plates (Figure 1). In this complex region, the South Caribbean tectonic evolution reflects the interaction between the Caribbean plate and the northwestern border of South America since Late Cretaceous times. As a consequence of this interaction different stress regimes prevailed as oceanic terranes were accreted against the continental margin, which resulted in mountain building. Three mountain belts of the northern Andes resulted from this process, the Eastern Cordillera of Colombia (EC hereinafter) is the easternmost belt (Figure 2). Apatite fission tracks data indicate thermal cooling sometime between 60 and 30 Ma, suggesting a pulse of uplifting of the EC during the Paleogene [*Gomez et al.*, 2003]. This deformation continued as an episodic process that culminated with the main Pliocene-Pleistocene Andean phase. The Neogene tectonic phase induced the tectonic inversion of the Late Jurassic to Cretaceous intracontinental basin [*Colletta et al.*, 1990; *Cooper et al.*, 1995; *Dengo and Covey*, 1993; *Sarmiento*, 2001].

[3] At the regional scale, the geometry of the Eastern Cordillera is characterized by NE-SW trends following in general the direction of basement-involved normal faults. However, this structural grain is neither continuous nor homogeneous and in places turns to N-S and even trends NNW-SSE (Figure 2). This variety of structural patterns may reveal (1) local variations in orientations of inherited basement structures, (2) local response of basement structures to stress regimes, or (3) syntectonic reorientation and rotation of basement structures to accommodate different stress regimes.

[4] The purpose of this study is to describe and to analyze the results of systematic measurements and determinations of paleostress in two regions of the EC which present different regional trends; N-S trend of the Guaduas Syncline and NE-SW trend of the Sabana de Bogotá (Figure 2). We characterize the Late Cretaceous and Cenozoic stress

[1]Now at Corporación Geológica Ares, Bogotá, Colombia.

0278-7407/05/2003TC001551

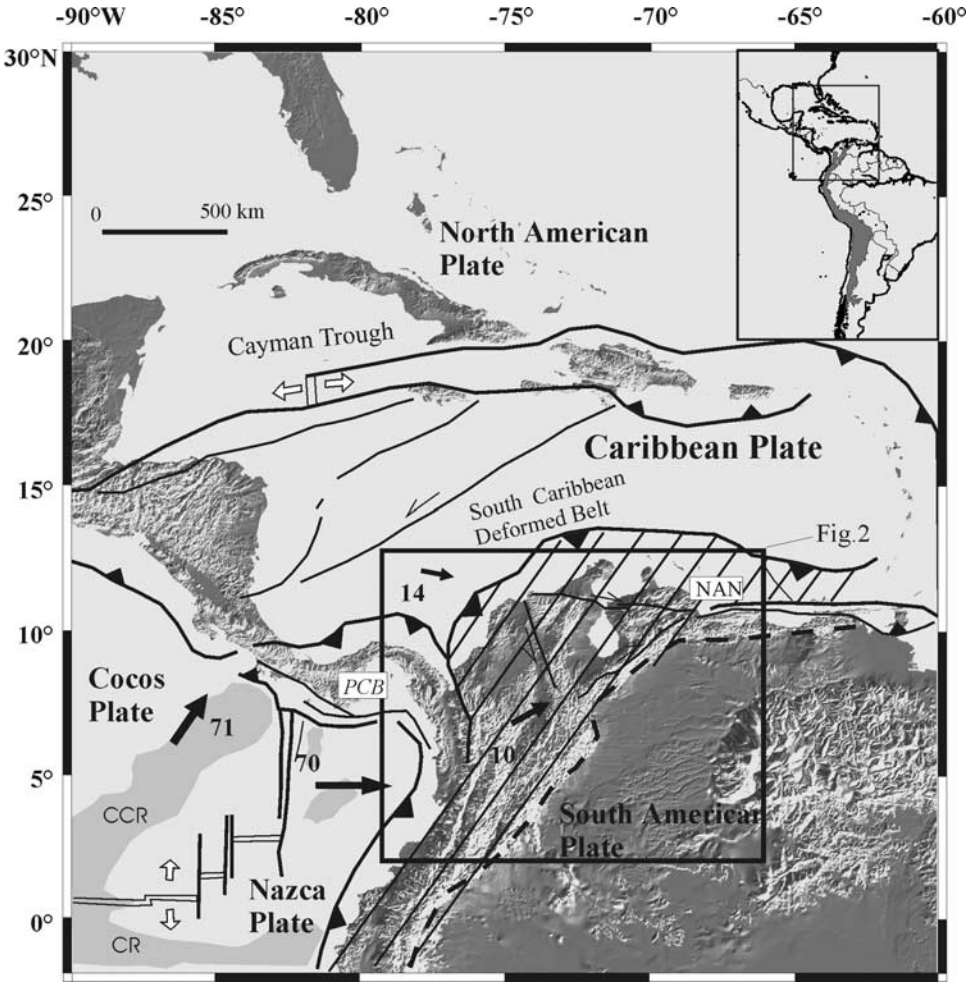

Figure 1. Tectonic elements of the NW South America. Abbreviations are as follows: NAN, North Andes Block (cross-hatched area); PCB, Panama-Chocó Block; CR, Carnagie Ridge; CCR, Cocos Ridge. Arrows and numbers are present-day velocity plates from *Freymueller et al.* [1993] in mm/yr with respect to South America.

regimes in these areas and we reconstruct a tectonic chronology based on crosscutting relationships of small-scale structures observed in the field. We finally explain this deformation history within the framework of the South Caribbean tectonic evolution. This is done through comparison of results obtained from our tectonic analyses and the paleostress sequence predicted using a revised kinematic model of this region. In addition we provide a synthesis of the sequence of tectonic regimes that has affected the northern Andes since Late Cretaceous times.

1.1. Plate Tectonics of the Caribbean Region

[5] The early tectonic evolution of the Caribbean region is related to breakup of Pangea and the subsequent separation of the plates of North America (NA) and South America (SA) [*Pindell and Dewey*, 1982]. The analyses of sea floor magnetic anomalies in the Atlantic Ocean allowed accurate reconstruction of rotation poles and relative displacement paths between the North America - Africa and Africa - South America. The reconstruction of the South America-North America relative displacements was carried out using finite rotation analysis [*Laad*, 1976; *Pindell*, 1985; *Pindell et al.*, 1988; *Pindell and Dewey*, 1982]. These results were updated by using the Atlantic Indian hot spot reference frame [*Müller et al.*, 1999].

[6] As a result, we know that the separation between the continental plates of NA and SA, as a consequence of the breakup of Pangea during the Jurassic, gave place to new oceanic crust in the Proto-Caribbean. This oceanic opening was coeval with the northeastward subduction of the oceanic crust of the Farallon plate (FA) [*Duncan and Hargraves*, 1984]. During the Late Cretaceous, the easternmost part of the Farallon plate became an independent plate, the Caribbean plate, which began to be inserted between the Americas [*Burke et al.*, 1984; *Pindell et al.*, 1988; *Pindell and Dewey*, 1982; *Ross and Scotese*, 1988]. This new oceanic plate was characterized by anomalous buoyancy [*Burke et al.*, 1978] which has been associated to its displacement above the Galapagos hot spot [*Duncan and Hargraves*, 1984]. The resulting thick

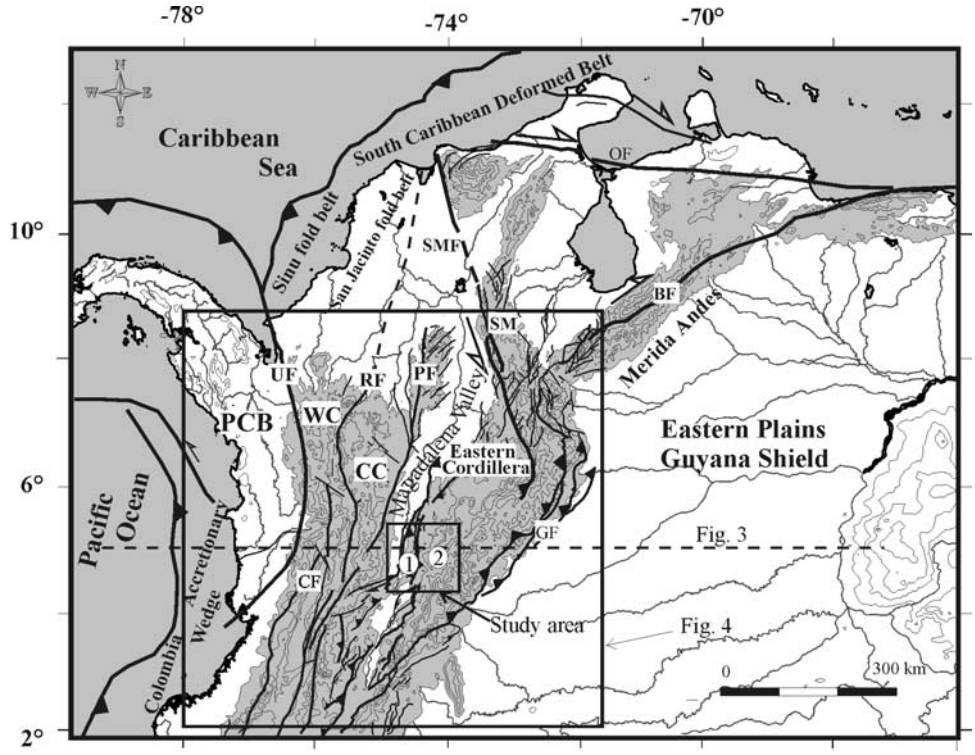

Figure 2. Main structural features of the northern Andes: Abbreviations are as follows: PCB, Panama-Chocó Block; UF, Uramita fault; WC, Western Cordillera; RFZ, Romeral fault zone; CF, Cauca-Patia fault; CC, Central Cordillera; PF, Palestina fault; SMF, Santa Marta-Bucaramanga fault; SM, Santander Massif; OF, Oca fault; BF, Boconó fault; GF, Guaicaramó fault. Circled numbers are 1, Guaduas Syncline; 2, Sabana de Bogotá.

oceanic plateau began to be inserted between the Americas as the proto-Caribbean and Atlantic Ocean subducted beneath it. As a consequence, the ocean floor of the Proto-Caribbean, including its magnetic anomalies which recorded the opening between the Americas, was definitively lost. The remnant FA plate became the Cocos plate (CC) and the Nazca plates (Nazca) during Miocene time [*Hey*, 1977].

[7] The insertion of the Caribbean plate between the Americas since the Late Cretaceous induced activation of large shear zones along the northern and southern edges of the Caribbean: the Cayman Trough in the northern edge, and the Oca, El Morón, and El Pilar fault zones to the south [*Burke et al.*, 1984]. This activation initiated a subduction complex in northwestern South America and in the South Caribbean deformed belt. This activation was later enhanced because of the change from relative divergence to convergence between the Americas since late Paleocene time [*Müller et al.*, 1999; *Pindell et al.*, 1988]. The effects of this relative convergence were of particular importance during the early Miocene time in the South Caribbean deformed belt in the basins of Colombia and Venezuela [*Müller et al.*, 1999].

1.2. Northern Andes: Present Tectonic and Kinematic Framework

[8] The northern Andes (Figure 1) are located in a region considered as a large triple junction under construction between the Nazca, South America, and Caribbean plates [*Ego et al.*, 1996]. This triple junction area behaves as an independent mobile block, which has been referred to as the North Andes Block [*Kellogg and Vega*, 1995; *Pennington*, 1981]. Geodetic (GPS) measurements suggest that the present movement of the north Andes as an escape block occurs toward the ENE relative to stable South America, which implies a dominant right-lateral transpressive behavior of faults bounding the eastern margin of the Eastern Cordillera of Colombia [*Freymueller et al.*, 1993; *Pennington*, 1981; *Trenkamp et al.*, 2002].

[9] This model of the northern Andes as a single mobile block escaping toward the ENE however involves some contradiction. Seismic data from the northern Andes area show that in the southern portion of the northern Andes the E-W convergence of the Nazca and South America plates induce a right-lateral stress regime that affects the faults bounding the Eastern Cordillera south of 4°N [*Ego et al.*, 1996]. This would be consistent with a model of ENE escape of the northern Andes. However, northward of 4°N the northern Andes region is mainly under influence of the Caribbean plate [*Ego et al.*, 1996; *Cortés*, 2004]. In this northern area, the focal mechanisms of earthquakes [*Corredor*, 2003; *Dimate et al.*, 2003; *Cortés*, 2004], the fault kinematic data [*Taboada et al.*, 2000] and the structural reconstructions of the eastern

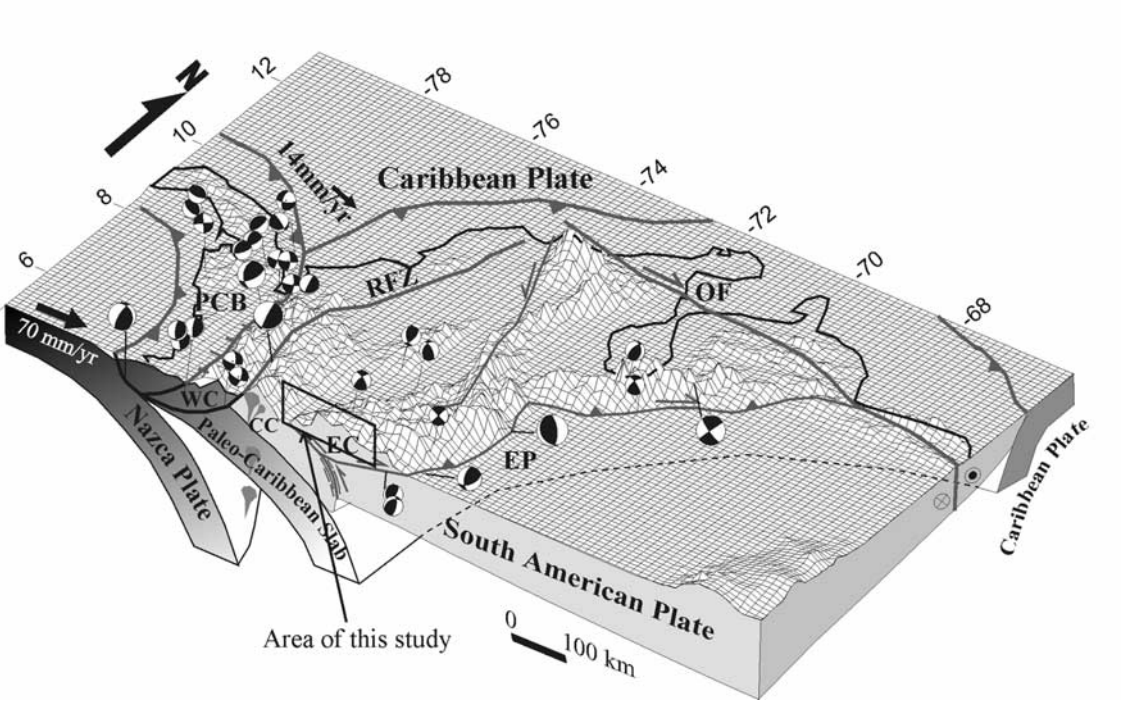

Figure 3. Present-day schematic cross section through the north Andes in Colombia. For location see Figure 2. Abbreviations are as follows: PCB, Panama-Chocó Block; WC, Western Cordillera; CC, Central Cordillera; EC, Eastern Cordillera; EP, Eastern Plains; RF, Romeral fault; OF, Oca fault. Adapted from *Colletta et al.* [1990], *Cortés* [2004], *Kellogg and Vega* [1995], *McCourt et al.* [1984], and *Taboada et al.* [2000]. Focal mechanisms from University of Harvard, CMT solutions.

flank of the Eastern Cordillera [*Branquet et al.*, 2002; *Casero et al.*, 1997; *Colletta et al.*, 1990; *Cooper et al.*, 1995; *Rowan and Linares*, 2000] revealed a rather compressive behavior on the eastern margin of the northern Andes between 4° and 8°N. Accordingly, the direction of maximum compression would be ESE there, rather than the transpression in the ENE direction as suggested by the GPS data. These considerations argue against a ENE displacement of the northern Andes in the northern segment of the Eastern Cordillera, and suggest that the accommodation of the deformation in the triple junction area is more complex than that involved by the a single block model.

[10] According to this kinematic pattern, in the northern Andes area, presently is being accommodate deformation associated to SE dipping subduction of the Caribbean beneath northwestern Colombia and the east dipping subduction of the Nazca plate in the western margin (Figure 2). The Panama isthmus, located between the Caribbean and Nazca plates, accommodates deformation related to convergence of these plates in an approximately N-S direction [*Kellogg and Vega*, 1995; *Pennington*, 1981].

[11] The present-day plate boundaries in this region remain uncertain because of the tectonic complexity and accretion of oceanic crust against the active continental margin. The geometry of subducted slabs is still controversial in NW Colombia as a consequence of the absence of magmatic arc and very scarce shallow seismicity associated to the subduction of the Caribbean plate in the northwestern Caribbean coast. However, the development of an accretionary prism is well documented [*Duque-Caro*, 1984; *Ruiz et al.*, 2000; *Toto and Kellogg*, 1992]. The distribution of intermediate to deep seismicity and associated focal mechanisms in the Perija Range, Merida Andes and northern EC have been used to demonstrate the presence of a north to NNW striking and east dipping slab beneath northern Colombia [*Dewey*, 1972; *Kellogg and Bonini*, 1982; *Malave and Suarez*, 1995; *Pennington*, 1981; *Taboada et al.*, 2000; *Toto and Kellogg*, 1992].

[12] *Pennington* [1981] observed that the intermediate to deep seismicity concentrates in well-defined areas that he used to define three slabs of oceanic crust subducting beneath the Andes in Colombia and NW Venezuela. He consequently defined the Bucaramanga segment related to the Caribbean plate and the Cauca and Ecuador segments associated to the Nazca plate. Tomographic images were later used to redefine and to confirm the presence of two slabs sinking below NW and W Colombia, respectively related to Caribbean and Nazca plates [*Gutscher et al.*, 2000; *Taboada et al.*, 2000; *Van der Hilst and Mann*, 1994]. *Taboada et al* [2000] suggested the presence of a remnant ancient paleo-Caribbean plate which subducts beneath the northern segment of the Eastern Cordillera. Figure 3 is

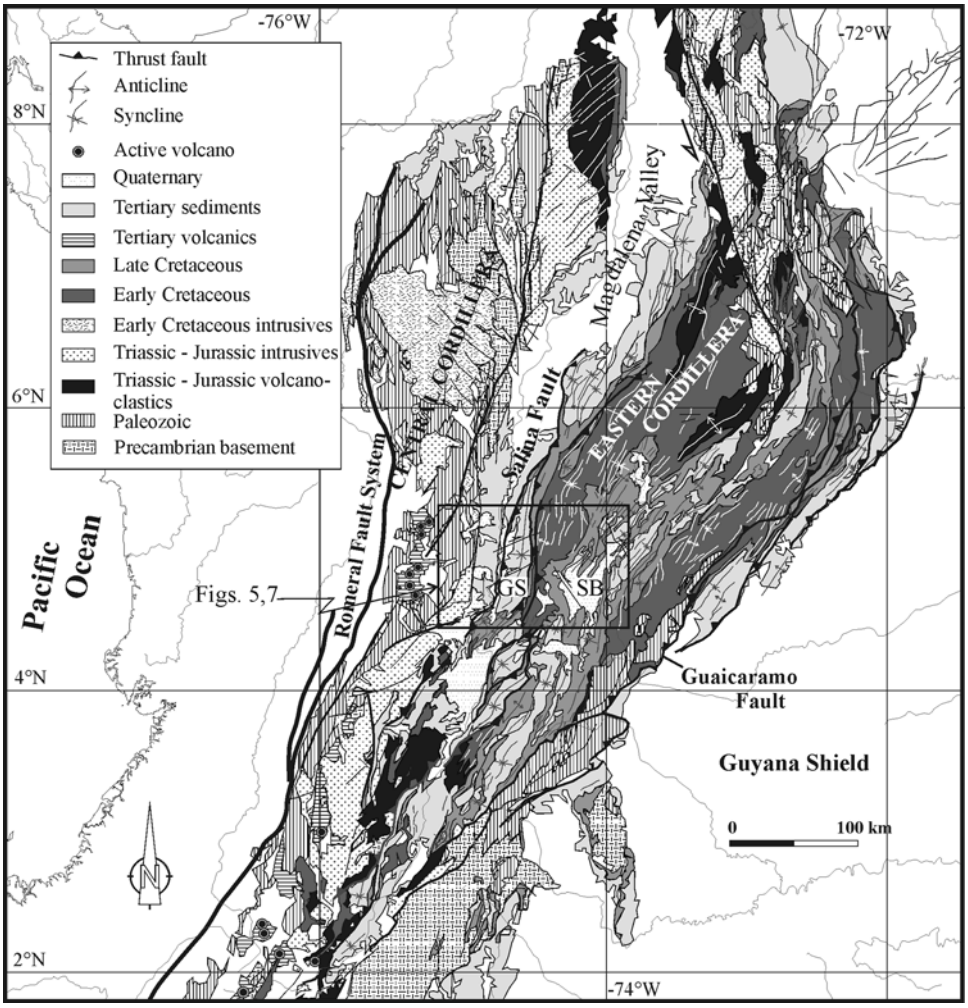

Figure 4. Generalized geological map of the Eastern Cordillera and the eastern flank of the Central Cordillera of Colombia. Modified from *Cediel and Cáceres* [1988], *Raasveldt* [1956], and *Raasveldt and Carvajal* [1957]. Abbreviations are GS, Guaduas Syncline; SB, Sabana de Bogotá.

a schematic diagram of the possible north Andes plate architecture.

1.3. Regional Geology of Colombia

[13] The Andean system in Colombia results from a polyphase history of deformation. Episodic processes of subduction-obduction and collisions have occurred in the western margin of Colombia since Precambrian times and continue until present day [*McCourt et al.*, 1984; *Restrepo-Pace*, 1995]. In consequence, three mountain belts have developed, namely, the Eastern Cordillera (EC), the Central Cordillera (CC), and the Western Cordillera (WC). East of the EC, and bounded by the Guaicaramo fault, the eastern plains overlie the stable Guyana shield (Figure 4).

[14] The basement underlying the EC and the eastern flank of the CC is composed of a Precambrian core of granulite facies metamorphic rocks, which resulted from a continent-continent type collision during the late Precambrian [*Kroonemberg*, 1982; *Restrepo-Pace*, 1995; *Restrepo-Pace et al.*, 1997]. These rocks are overlain by a sequence of amphibolite facies metamorphic rocks of marine sedimentary origin, produced during Ordovician time (Caparonensis Orogeny) [*Restrepo-Pace*, 1992, 1995]. Locally, this core of metamorphic rocks is unconformably overlain by folded late Paleozoic marine sediments [*Villarroel and Mojica*, 1987]. The entire sequence is intruded by granitic-type batholiths of Late Jurassic to Early Cretaceous age that developed in response to continuous east dipping subduction of the oceanic crust of the FP under NW South America [*Restrepo-Pace*, 1995]. This metamorphic and crystalline basement crops out in EC as cores of giant anticlines that are observable in the Garzón-Quetame and the Santander massifs and constitutes the bulk of the CC and Santa Marta Range [*Jullivert*, 1970] (Figure 4).

[15] According to geophysical and gravimetric observations [*Case et al.*, 1971, 1973; *Meissnar et al.*, 1976], the western flank of the CC, the WC and the Baudó Range (BR) are composed of oceanic-affinity crust which resulted from

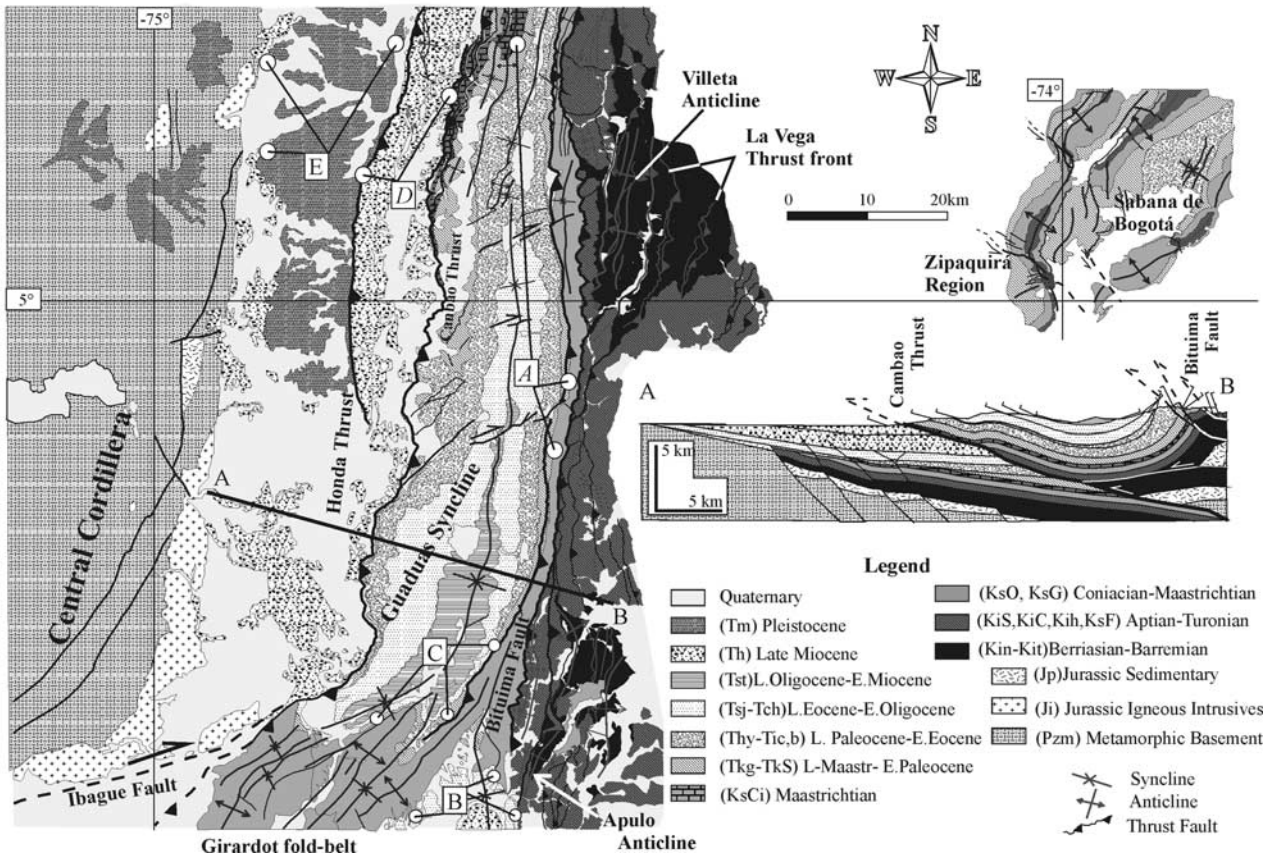

Figure 5. Geological map of the study area and key cartographic features that constrain timing of deformation in the western flank of the EC. Geology of the Central Cordillera and SW tip of the Girardot fold belt modified after *Raasveldt* [1956] and *Raasveldt and Carvajal* [1957]. Features are labeled as follows: A, in the eastern flank of the Guaduas Syncline, the absence, facies change, and wedging of the Cimarrona Formation evidence syntectonic sedimentation during the late Maastrichtian; B, in the Apulo Anticline area, posttectonic middle to late Eocene conglomerates (Chicoral Formation), unconformably overlie folded and faulted Cretaceous beds, suggesting premiddle Eocene activity of the Bituima thrust-fault; C, in the eastern flank of the Guaduas Syncline, the base of the posttectonic middle to upper Eocene conglomerates (San Juan de Rio Seco Formation), wedges out the upper Paleocene unit (Hoyón Formation) and rests on Lower Paleocene strata, highlighting postearly Eocene folding; D, upper Miocene units affected by major thrust faults in the western flank of the EC evidence post-late Miocene Andean tectonic activity; E, tilted beds of the Pliocene Mesa Formation unconformably rest on faulted beds of the late Miocene Honda Formation indicating post-Pliocene deformation.

multiple accretion episodes since the late Paleozoic [*McCourt et al.*, 1984; *Restrepo-Pace*, 1992, 1995]. These rocks include pelagic sediments, turbidites, basalts and volcanics as well as ultramafic and mafic intrusives, ranging in age from Early to Late Cretaceous [*Alvarez and Gonzalez*, 1978; *Barrero*, 1979; *Bourgois et al.*, 1982, 1987; *Etayo-Serna et al.*, 1982]. Meso-Cenozoic calcalkaline granitoid intrusive bodies intrude the CC, WC and BR. Their relative ages reveal migration of magmatism toward the west during Meso-Cenozoic times and toward the East later during Cenozoic times [*Alvarez*, 1983]. The limit between the accreted oceanic crust and the continental deformed margin is the Romeral fault, the tectonic complex history of which is closely related to processes of accretion and reveals periods of normal, inverse and strike-slip faulting [*Barrero*, 1979]. This fault zone is now the site of active seismicity (Figures 2, 3, and 4).

[16] Plutonism and volcanism resulting from continuous subduction during the late Jurassic to Early Cretaceous was localized in the present area of CC and Magdalena Valley (MV) as an active magmatic arc. In contrast, back arc type basins were emplaced in the area of the EC, where tectonic and then thermal subsidence controlled deposition of a sequence of continental to shallow marine sediments that reached a thickness of up to 9 km in the axial zone of the EC [*Fabre*, 1987; *Sarmiento*, 2001].

[17] Uplifting of the Central Cordillera began in the Late Cretaceous as a consequence of accretion of the WC [*Cooper et al.*, 1995] and tectonic inversion of the Eastern Cordillera began in Paleogene [*Colletta et al.*, 1990; *Gomez*

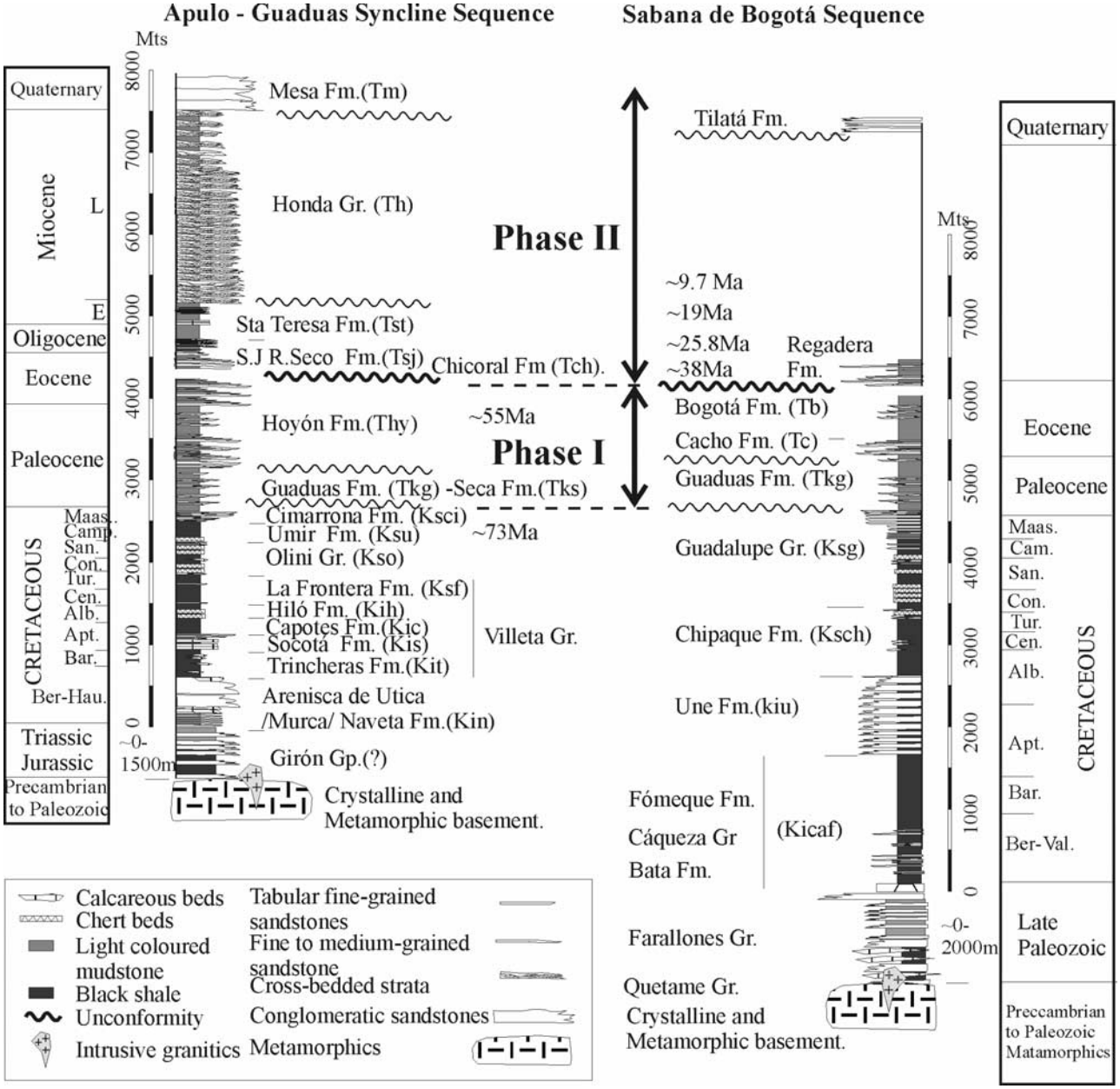

Figure 6. Lithostratigraphic diagram of units in the western flank and axial zone of the EC, as discussed in this paper. Modified after *Cáceres and Etayo-Serna* [1969], *Cortés* [2004], and *Sarmiento* [1989].

et al., 2003]. It continued as an episodic process that culminated in the late Miocene to the Recent, in response to continent-oceanic arc collision of the Chocó-Panamá arc [*Duque-Caro*, 1990; *Taboada et al.*, 2000]. During Neogene times, the Andean tectonic phase induced a compressive stress regime in the area of the ancient back arc basin. The inversion of the EC basin thus resulted in a major pop-up type structure, elongated according to the trend of the ancient normal faults. Development of large foreland basins on both flanks of this major pop-up structure accompanied the uplift of the EC, where deposition of Tertiary synorogenic sediments took place [*Casero et al.*, 1997; *Colletta et al.*, 1990; *Cooper et al.*, 1995].

[18] In the study area, the main faults accounting for uplifting along the western flank of the EC are, from east to west, La Vega, Bituima, Cambao and Honda thrusts (Figure 5). In general terms, these faults were formed in a sequence of faulting advancing from east to west. In consequence, La Vega thrust front is the earliest and internal fault, whereas the Honda thrust is the most recent and external one. Some periods of out-of-sequence and reactivation of earlier faults, however, affected this sequence of faulting [*Cortés*, 2004].

[19] In this study, particular emphasis is put on the analyses of deformation of sedimentary rocks in the EC. We especially considered the western portion of the EC,

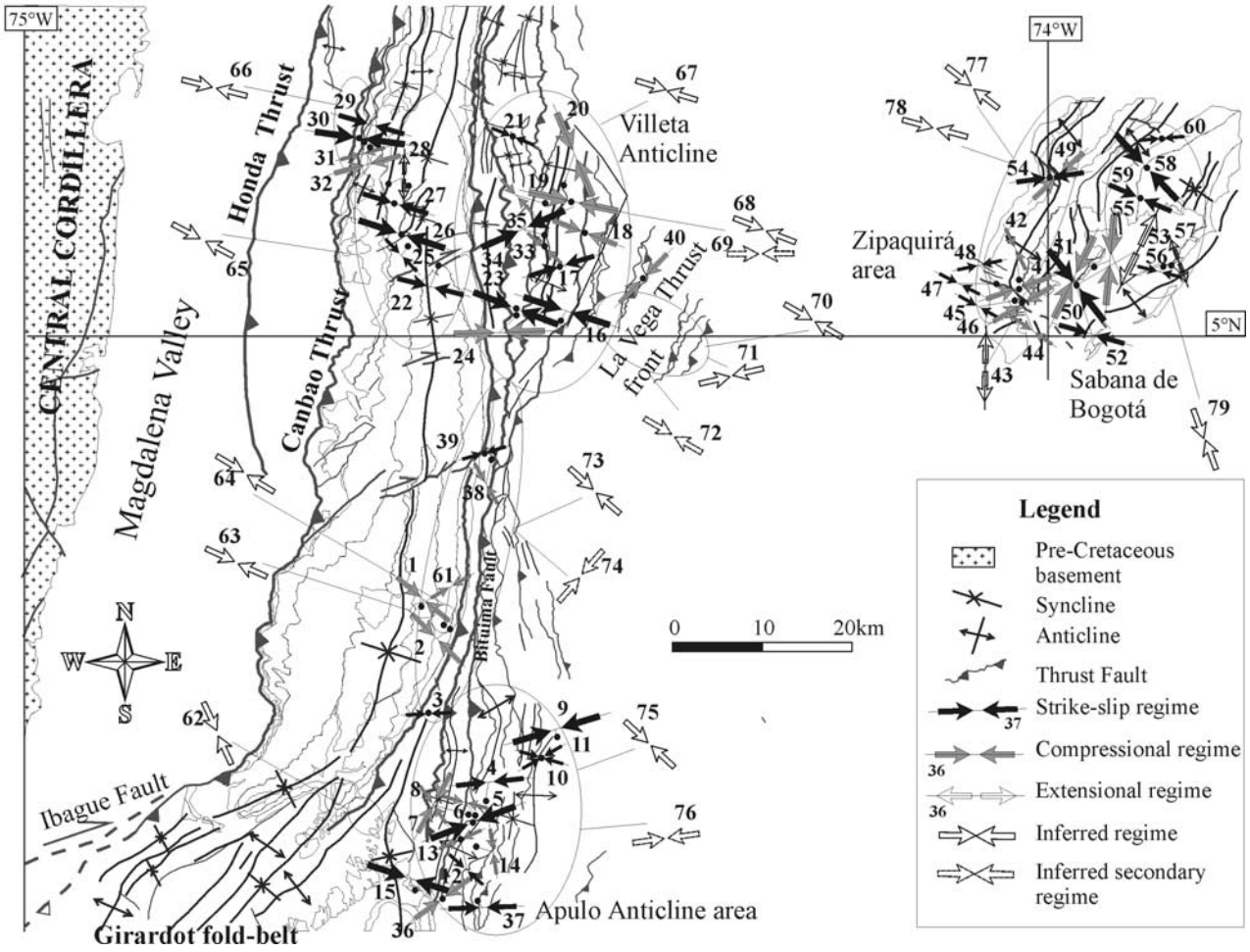

Figure 7. Tectonic map of the studied area showing the more relevant structural determinations. Gray and black arrows correspond to horizontal projection of contraction directions from fault slip data analyses presented in Table 1 and Figures 11a–11b. White arrows are geometrically deducted stress patterns.

where lower Cretaceous to the Miocene rocks crop out. These rock units have recorded deformation related to the Late Cretaceous accretion of the WC and paleostress associated to early uplifting of the EC, as well as the episodic Paleogene belt growth and finally the Neogene main Andean tectonic phase. Figure 6 summarizes the main stratigraphic features of the Western flank and axial zone of the EC, in the Guaduas Syncline and Sabana de Bogotá areas respectively.

2. Timing of the Deformation in the EC, Evidence From Synorogenic Sediments

[20] Figure 5 shows the more relevant geologic features of the studied regions and the areas where field mapping was focused. Figure 7 shows the sites used for brittle tectonic analysis. Preliminary conclusions concerning the timing of tectonic pulses are from both geometrical observation (i.e., crosscutting relationships between structures) and considerations about the distribution of unconformities. Relationships between syntectonic units of Tertiary age and structures in the area of the Guaduas Syncline allowed us to constraint the history of tectonic pulses affecting the EC.

2.1. Late Maastrichtian-Paleocene Pulse

[21] The Maastrichtian conglomeratic deposits (Cimarrona Formation, Figure 6) are usually considered as evidence of the first tectonic activity of the CC [*Gomez et al.*, 2003; *Gomez and Pedraza*, 1994; *Raasveldt and Carvajal*, 1957]. In the western flank of the Guaduas Syncline (Figures 5 and 6), these deposits are 80–100 m thick, and consist of coarse grained to conglomeratic beds below the Late Maastrichtian to Paleocene Guaduas Formation. In contrast, in the eastern flank of the same structure, these beds are absent and the fine-grained Late Maastrichtian to Paleocene unit (Guaduas Formation, Figure 6) paraconformably overlies the sequence of Campanian-Maastrichtian black shales (Umir Formation, Figure 6). *Gomez et al.* [2003] observed an eastward wedging of the coarse-grained Maastrichtian unit and they correlated it with a 15 m thick limestone in the eastern flank of the Guaduas Syncline. This highlights a late Maastrichtian syntectonic character of

Table 1. Numerical Values of Paleostress Determinations in the Eastern Cordillera[a]

No.	Stop	Latitude	Longitude	Unit	Age	σ1	σ2	σ3	Φ	Faults	Quality
1	33	04°43′04″	74°36′56	Tsj	L.Eocen-Olig.	310/16	44/14	172/68	0.45	10	B
2	66-57	04°42′32″	74°34′33″	Thy-Ku	L.Cret-Eoc	314/2	45/9	214/81	0.57	20	B
3	109	04°38′03″	74°36′33″	KsCi	Maastrichtian	87/19	251/70	355/5	0.33	11	C
4	115	04°32′41″	74°33′00″	KiS	Aptian	84/13	229/74	352/9	0.24	13	B
5	127-136b-139	04°31′43″	74°33′48″	Kis,Kic,Kin	Valang-Aptian	69/37	280/49	172/16	0.57	20	A
6*	136a	04°31′43″	74°33′48″	Kis	Aptian	105				6	C
7	132a-135a	04°32′01″	74°33′45″	Kis	Aptian	29/5	120/7	264/81	0.32	8	B
8	132b-135b	04°32′01″	74°33′45″	Kis	Aptian	325/15	234/4	131/75	0.52	6	C
9	156	04°36′11″	74°29′1″	Kit	Barremian	73/1	214/89	343/0	0.68	16	A
10*	160a	04°35′40″	74°29′30″	Kit	Barremian	106				4	C
11	160b	04°35′40″	74°29′30″	Kit	Barremian	240/28	77/61	333/7	0.32	6	C
12	168a	04°30′35″	74°34′22″	Kin	Valanginian	132/8	266/79	40/8	0.45	4	C
13	168b-172a	04°30′35″	74°34′22″	Kin	Valanginian	246/18	338/7	87/71	0.66	4	C
14	170–172	04°30′00″	74°33′22″	Kis,Kin	Aptian-Valang.	352/17	260/4	156/73	0.35	14	C
15	195	04°27′27″	74°37′11″	Tsj	L.Eocen-Olig.	288/1	23/76	198/14	0.31	17	A
16	221	05°01′05″	74°28′54″	Kin	Valanginian	108/6	236/80	18/8	0.6	15	A
17	232,245,265,275	05°04′47″	74°28′46″	Kin	Valanginian	73/2	210/88	343/1	0.29	27	B
18	245a,246,250	05°06′02″	74°27′16″	Kit	Barremian	111/0	203/77	21/13	0.12	29	B
19	253255256	05°07′32″	74°27′33″	Kin	Valanginian	102/1	12/0	264/89	0.48	12	A
20	264,299a	05°08′59″	74°28′02″	Kin,Kih	Albian-Valang.	157/2	66/14	257/76	0.62	22	A
21	299b	05°11′35″	74°31′33″	Kih	Albian	112/7	360/73	204/16	0.17	13	C
22	346	05°03′59″	74°35′41″	Tsj	L.Eocen-Olig.	284/16	61/68	190/14	0.07	9	B
23	317c,319b	05°01′36″	74°31′22″	Kis	Aptian	291/2	130/88	21/1	0.47	26	A
24	317b,319a	05°01′17″	74°31′15″	Kis	Aptian	268/6	359/14	156/75	0.12	22	A
25	349	05°05′33″	74°37′15″	Thy	Paleoc-E.Eocen	316/4	224/30	53/60	0.02	14	C
26	351	05°05′57″	74°37′41″	Thy	Paleoc-E.Eocen	288/23	138/63	23/12	0.47	31	A
27	357	05°07′47″	74°38′29″	Thy	Paleoc-E.Eocen	287/37	196/1	104/53	0.1	7	B
28	358,359a	05°08′48″	74°38′49″	Thy	Paleoc-E.Eocen	288/70	95/14	1/2	0.34	9	C
29	365	05°11′22″	74°40′16″	Ksc	Maastrichtian	286/33	54/43	175/29	0.19	7	B
30	363,367	05°11′41″	74°40′30″	Ksc	Maastrichtian	98/3	3/61	189/29	0.51	11	A
31	364,366	05°11′15″	74°40′04″	Ksc	Maastrichtian	75/9	166/7	293/79	0.68	14	C
32	361	05°11′07″	74°39′46″	Ksc	Maastrichtian	75/3	345/9	186/81	0.26	8	B
33*	378	05°06′43″	74°29′40″	Kin	Valanginian	132				6	C
34	379	05°06′22″	74°29′39″	Kin	Valanginian	246/11	360/64	152/23	0.03	18	A
35	380	05°07′04″	74°29′10″	Kin	Valanginian	137/9	43/24	247/64	0.88	8	C
36	384,388	04°26′49″	74°35′18″	Kih	Albian	234/0	144/1	326/89	0.28	10	B
37	388a	04°27′05″	74°33′47″	Kih	Albian	268/25	66/64	174/9	0.23	7	C
38	401,405	04°52′47″	74°32′41″	Kso	Santonian	150/6	241/11	34/77	0.66	10	C
39	402	04°53′13″	74°33′00″	Ksu	Maastrichtian	74/12	316/66	168/21	0.75	14	C
40	436	04°03′14″	74°23′23″	Kit	Barremian	44/1	314/15	138/75	0.38	6	B
41	511	05°02′42″	74°01′43″	Ksg	Campanian	251/0	341/14	161/76	0.02	12	B
42*	514	05°03′18″	74°01′52″	Ksg	Campanian	327				9	C
43	506a	05°01′51″	74°01′29″	Ksg	Campanian	34/73	273/9	181/14	0.16	6	B
44	506c	05°01′51″	74°01′29″	Ksg	Campanian	125/9	217/12	357/75	0.24	5	C
45	518a	05°01′59″	74°02′16″	Ksg	Campanian	119/2	222/79	28/11	0.63	5	C
46	506b,518b	05°01′59″	74°02′16″	Ksg	Campanian	239/15	146/11	20/71	0.4	9	B
47*	520a	05°02′56″	74°02′59″	Ksg	Campanian	297				7	C
48	520b	05°02′56″	74°02′59″	Ksg	Campanian	258/4	12/81	167/9	0.48	4	C
49	523,525	05°09′47″	74°59′50″	Ksg	Campanian	227/7	137/0	44/83	0.28	12	B
50	546a,547	05°10′05″	74°00′20″	Ksg	Maastrichtian	206/6	301/44	110/46	0.25	14	A
51	546b	05°10′05″	74°00′20″	Ksg	Maastrichtian	322/2	225/74	53/16	0.08	16	A
52	546c	05°10′05″	74°00′20″	Ksg	Maastrichtian	106/19	340/60	204/23	0.32	9	B
53	546d	05°10′05″	74°00′20″	Ksg	Maastrichtian	266/81	116/7	26/4	0.49	9	A
54	543	05°09′40″	73°59′40″	Ksg	Maastrichtian	82/2	195/84	352/6	0.4	6	B
55	549	05°03′13″	73°58′02″	Ksg	Maastrichtian	185/29	320/52	82/23	0.12	9	A
56	555	04°04′10″	73°53′03″	Ksg	Maastrichtian	104/11	238/74	11/11	0.73	6	C
57	556	04°04′04″	73°52′49″	Ksg	Campanian	74/60	249/30	340/2	0.38	10	C
58	570	04°09′43″	73°54′03″	Tic	E.Eocen	137/4	10/83	227/6	0.1	12	A
59	568,569	05°07′25″	73°54′36″	Tic	E.Eocen	113/8	225/70	20/18	0.22	12	B
60	572	05°11′35″	73°53′06″	Ksg	Maastrichtian	265/15	37/69	171/15	0.44	8	C
61	54,64,66,69	04°42′56″	74°35′11″	Thy-Tkg	L.Paleoc-Eoc	240/12	331/7	91/76	0.59	23	C
	Other Structures[b]	Stop	Latitude	Longitude	Unit	Age	σ1	σ2	σ3	No. Data[c]	Quality
62	198–215	04°31′53″	74°39′22″	Kso	Coniac-Maast.	155				46	C
63	30-43	04°43′08″	74°36′47″	Tsj	L.Eocen-Olig.	115				48	C
64	45-64, 64-72	04°42′52″	74°35′11″	Thy	Paleoc-E.Eocen	121				72	C
65	335-359	05°05′27″	74°37′06″	Thy-Tjs	L.Paleo-Oligoc	118				72	C
66	361-369	05°11′16″	74°40′06″	KsCi	L. Cretaceous	104				67	C

Table 1. (continued)

	Other Structures[b]	Stop	Latitude	Longitude	Unit	Age	σ1	σ2	σ3	No. Data[c]	Quality
67	220-296	05°06′22″	74°29′39″	Kin-Kit-Kis	E.Cretaceous	107				238	C
68	220-297	05°06′22″	74°29′39″	Kin-Kit-Kis	E.Cretaceous	111				100	C
69	220-298	05°06′22″	74°29′39″	Kin-Kit-Kis	E.Cretaceous	90				26	C
70	421-447	05°03′50″	74°24′25″	Kin-Kit	E.Cretaceous	120				134	C
71	421-448	05°03′50″	74°24′25″	Kin-Kit	E.Cretaceous	77				50	C
72	421-449	05°03′50″	74°24′25″	Kin-Kit	E.Cretaceous	120				30	C
73	1-109	04°40′16″	74°34′56″	Kso	Coniac-Maast.	131				56	C
74	1-110	04°40′16″	74°34′56″	Kso	Coniac-Maast.	42				15	C
75	114-184,384-391	04°30′00″	74°33′22″	K..	Cretaceous	133				51	C
76	114-184,384-392	04°30′00″	74°33′22″	K..	Cretaceous	82				19	C
77	500-545	05°02′42″	74°01′43″	Ksg	Coniac-Maast.	128				32	C
78	500-545	05°02′42″	74°01′43″	Ksg	Coniac-Maast.	105				75	C
79	546-578	04°03′39″	74°52′02″	Ksg-Tc-Tb	Coniac-Eocene	161				62	C

[a]Quality factors are labeled as follows: A, fair quality determination, with stress tensor reasonably constrained by data; B, average quality; C, poor quality determination. Reference numbers with asterisks refer to situations without significant stress tensor being determined (in these cases, only the probable azimuth of compression is shown with a single number in columns σ1, σ2, and σ3, and an open arrow in Figure 11b). Stress axes indicated in terms of azimuth and dip angle in degrees. $\Phi = (\sigma 2 - \sigma 3)/(\sigma 1 - \sigma 3)$.

[b]Structures other than fault striated planes, i.e., styolites, slaty cleavy, joints, etc.

[c]Number of field measures constraining the stress determination.

sedimentation. According to our mapping, this tectonic episode especially affected the eastern flank of the Guaduas Syncline (Point A in Figure 5).

2.2. Late Paleocene–Early Eocene Major Deformation

[22] One of the most important features within the Tertiary record of Colombia is the late Paleocene–Eocene unconformity. This unconformity is locally high-angle in type in the Magdalena Valley to paraconformable in the Llanos basin [*Restrepo-Pace*, 1999; *Villamil et al.*, 1995]. We paid special attention to structures and sediments related to this unconformity because of its regional importance for the structural development of the EC.

[23] The precise age of Cenozoic deposits in the Guaduas Syncline is a matter of debate. In the Tertiary sequence of this structure, the first coarse-grained unit is the Hoyón Formation. This unit is locally a 1000-m-thick conglomerate (Figure 6), dated as early Eocene [*Van der Hammen*, 1958] and early Oligocene [*Porta and de Porta*, 1962] or older than the late Paleocene-early Eocene unconformity [*Gomez et al.*, 2003; *Sarmiento*, 2001]. Analysis of one palynologycal sample of this unit collected in the field station of stress determination 2 (Figure 7 and Table 1) resulted in a Paleocene-early Eocene (?) age (C. Jaramillo and M. Rueda, ICP-Ecopetrol, personal communication, 2003).

[24] At the southern tip of the mapped area, the late Paleocene - Eocene unconformity is evidenced by the basal contact of the conglomeratic Chicoral Formation (Figures 5 and 6), dated as middle to late Eocene in the Upper Magdalena Valley [*Osorio et al.*, 2002]. These conglomerates overlie Cretaceous beds of different ages and involved different structures (Point B in Figure 5). In the mentioned area, the Bituima thrust fault and associated Apulo Anticline, involving Early Cretaceous units, are unconformably overlain by the Chicoral Formation conglomerates. In the footwall block of the Bituima thrust fault, the Chicoral Formation unconformably overlie the Upper Cretaceous Frontera and Lidita Inferior formations. Our field mapping confirms the earlier observation made by *Cáceres and Etayo-Serna* [1969] and *Cáceres et al.* [1970] in the same area. Consequently, deposition of the Chicoral Formation conglomerates postdates the activity of the Bituima thrust fault and the Apulo anticline, indicating a late pre-Eocene age for these structures (Point B in Figure 5).

[25] Angular unconformities related to deformation during the Eocene were detected at the southern tip of the Guaduas Syncline. At that place, subvertical beds of the late Paleocene–early Eocene Hoyón Formation pinch out and are unconformably overlain by the late Eocene-Oligocene San Juan de Rio Seco Formation which dips about 50° to the west (Figure 5). Southward of this locality the late Eocene-Oligocene strata unconformably overlie the Maastrichtian to early Paleocene mudstones of the Seca Formation (Point C of Figure 5). This structural pattern not only confirms the post late Paleocene-early Eocene deformation, but also provides geometrical evidence for continuing folding of the Guaduas Syncline, as a consequence of westward displacement on the Cambao fault since late Maastrichtian. Our field mapping of this area confirms the results from *Raasveldt* [1956] and *Porta* [1965] concerning the geometry of this unconformity.

[26] *Villamil et al.* [1995] explained the origin of the Paleocene-Eocene unconformity in terms of deformation associated with uplifting of the Central Cordillera followed by creation of a foreland type basin. In this model, deposition of fine-grained sequences occurred during periods of tectonic relaxation after a phase of strong tectonic activity and erosion. In contrast, deposition of coarse-grained deposits occurred during periods of relative tectonic quiescence (posttectonic deposits). Foreland subsidence was partially controlled by a remnant of the Upper Cretaceous thermal subsidence [*Sarmiento*, 2001]. Following this model, we consider the fine-grained Seca Formation as a sedimentary record of a period of high tectonic subsidence after a strong period of erosion affecting the Maastrichtian Cimarrona

Formation in the western flank of the Guaduas Syncline. This deformation was followed by deposition of a posttectonic conglomeratic unit; the Hoyón Formation which overlie paraconformably the Seca Formation (Figure 6).

[27] Alternatively, *Gomez et al.* [2003] assigned a Paleocene age to the entire sequence of the Hoyón Formation and included the Hoyon and Seca Formations (Guaduas Formation) as a single Late Cretaceous - Paleocene transgressive sequence. These authors argued that in the eastern flank of the Guaduas Syncline the conglomeratic Hoyón Formation interfingers with the muddy Seca Formation. This interpretation is supported with a seismic profile of the Guaduas Syncline where the base of the Hoyon Formation in the axial fold zone apparently coincides with the surface outcrop of the Seca Formation in the eastern flank (see Figure 6 of *Gomez et al.* [2003]). However, our field mapping in this area shows that the conglomeratic Hoyón Formation is deposited above the Seca Formation in both flanks of the Guaduas Syncline. In particular, in the eastern flank of this structure, the Cretaceous and Tertiary sequences are affected by a west verging thrust fault that overturns the conglomerate as well as the Seca Formation, displacing both units to the west. As a consequence, the fault omitted by *Gomez et al.* [2003] in the eastern flank of the Guaduas Syncline, explains the coincidence of the Hoyón and Seca Formations in this area through a simple thrust fault, rather than a lateral transition between conglomerates and mudstones (Figure 5, structural cross section).

[28] To summarize, a single late Paleocene - early Eocene regional tectonic phase appears to be responsible for the development of the main unconformity, as previously suggested by studies of *Villamil et al.* [1995] and *Gomez et al.* [2003]. Our field mapping, showing ancient fold-and-thrust structures and tilted beds fossilized below the unconformity, confirms these views. The origin of this unconformity has been associated with deformation in the Central Cordillera, which records the eastward displacement of the Caribbean plate and the diachronous accretion of the Panama Arch [*Villamil et al.*, 1995]. However, *Taboada et al.* [2000] suggest that this tectonic phase correlates well with the Paleogene accretion of the San Jacinto Terrane in northern Colombia as defined by *Duque-Caro* [1984].

2.3. Andean Tectonic Phase

[29] The most evident tectonic phase in the study area is the Andean Phase. In this region, the largest thrust fault of the western flank of the EC is the Cambao Thrust fault (Figure 5). This fault places the Upper Cretaceous rocks on top of the upper Miocene Honda Formation and transfers some of its displacement on the leading Honda thrust fault, which locally repeats the Eocene to late Miocene sequence. This fact clearly evidences a postlate Miocene phase accounting for more than 5 km of vertical displacement. (Point E of Figure 5).

2.4. Post-Andean Continued Deformation

[30] Post-Andean deformation seems to affect the western foreland basin of the EC. West of the Honda fault, the Pliocene Mesa Formation [*Raasveldt and Carvajal*, 1957] unconformably overlies tilted conglomeratic beds of the upper Miocene Honda Formation (Point D of Figure 5).

2.5. General Considerations on the Tectonic Phases of the Study Area

[31] On the basis of considerations of syntectonic sediments geometry and associated unconformities, it is thus possible to identify periods of folding and faulting that account well for the early development of structures in the western flank of the EC during the late Maastrichtian, late Paleocene to Eocene, as well as a major phase of faulting and folding that postdates the late Miocene Andean phase. Continued post-Andean deformation appears to be active. These results are summarized in the stratigraphic column of Figure 6, which shows unconformities between units.

[32] Our observations are in agreement with most previous works, accounting for continued deformation of the EC in regions outside the study. The early pre-Andean rising of the EC has already been documented by *Colletta et al.* [1990] who attributed wedging of the Paleogene sequence along the Salina thrust fault (Figure 4) as a result of an early pulse along this structure during the growth of the EC in the Middle Magdalena Valley. *Casero et al.* [1997] recognized four events preceding the Miocene Andean phase: a Late Cretaceous-lower Paleocene (Laramide I) phase that generated double verging thrust folds in the EC, an late Eocene-Oligocene phase (Laramide II)-, and two Miocene pre-Andean Phases. *Villamil* [1999] considered eastward depocenter migration in the foreland basin of the EC from Maastrichtian to Oligocene as a process linked to uplifting of the Central Cordillera. This model predicts early development of the EC occurring during the Oligocene. In the Middle Magdalena Valley, *Restrepo-Pace* [1999] reported a fold-and-thrust-belt structure below the late Paleocene-early Eocene unconformity evidencing development of late Paleocene to early Miocene structures related to the growth of the EC. *Gomez et al.* [2003] recognized two phases of folding during middle Eocene-Oligocene and late Miocene, prior to the main Andean phase in the Guaduas Syncline region. This pre-Andean phase is also reconstructed in the Upper Magdalena basin. fault activity during deposition of Eocene-Oligocene (Gualanday Group) and the Miocene (Honda Formation) was previously identified by [*Amezquita and Montes*, 1994]. On the basis of flexural models and evidence such as the presence of Paleogene unconformities, lateral changes of facies and thickness, local erosion indicated by detrital composition of sandstone and fission track data, *Sarmiento* [2001] suggests that an incipient inversion of Mesozoic extensional basins occurred since Paleogene times.

3. Paleostress Analysis

3.1. Methods and Assumptions

[33] Intraplate compressional deformation associated to active margins, as in the northern Andes, is subjected to interaction between at least two plates. This interaction is maximum at the plate boundary zone and it can cause intraplate deformation at distances of up to 1600 km

[*Ziegler et al.*, 1998]. Stress in such areas is accommodated as permanent deformation and large displacements along faults and microblocks. Structures and type of deformation along these areas is also a function of the directions of convergence and the degree of obliquity between major plates, as well as the geometry of the plate boundary and rheological properties of major structural units [*Hu et al.*, 1996]. It is thus possible and rather frequent to observe strain partitioning and strain deflection along plate boundaries in active margins. Strain measurements in such areas should reflect a complex pattern that is rarely parallel to directions of convergence between major plates. This is the case of the western boundary of the northern Andes. In this complex region, stress related to the triple junction between the oceanic Nazca and Caribbean plates and the continental South American plate is accommodated along the Panama-Chocó Block and most of the faults and structures around the Baudo Range and the Western Cordillera, including the Romeral and Uramita faults [*Cortés*, 2004; *Ego et al.*, 1996; *Kellogg and Vega*, 1995]. Such complexity is reflected in the distribution of focal mechanism of earthquakes showing a high variety of kinematic solutions in the area to the west and around of the Romeral fault zone (Figures 2 and 3). In southern Colombia and Ecuador, the E-W convergence of the Nazca plate is oblique with respect to the ENE-WSW faults of the northern Andes (southward of 4°N) inducing right lateral displacement on the major faults of the northern Andes [*Cortés*, 2004; *Ego et al.*, 1996; *Trenkamp et al.*, 2002].

[34] On the other hand, in the internal part of the continental plate, (eastward of the Romeral fault zone) deformation related to subduction of the Caribbean plate and its mechanical coupling with the South American plate seems to be less complex and strain patterns seem quite homogeneous [*Cortés*, 2004]. Focal mechanism of earthquakes showing in most cases compressive solutions associated to NE-SW to N-S trending faults in the northern portion of the Eastern Cordillera (Figure 3), suggest a homogeneous strain pattern in the internal part of the continental plate. Such homogeneity is compatible with geodynamic models of continental subduction below the Eastern Cordillera, proposed to account for the structure of this mountain belt [*Colletta et al.*, 1990; *Sarmiento*, 1989; *Taboada et al.*, 2000]. In such models, the subducted slab, which plunges beneath EC, transmits directly the stress related to subduction to the continental plate and hence to the EC through a ductile shear zone (Figure 3). Consequently, seismic patterns below the EC allow to assume that the strain measurements deducted from our study reflect a more direct interaction between the oceanic (Caribbean) subducted slab and the continental block of NW South America, and not a secondary strain pattern as could be the case of a complex plate boundary. In addition, the low degree of obliquity between the direction of convergence of the Caribbean plate (WNW-ESE) and major faults of the northern Andes (NNE-SSE), also suggests a low degree of strain deflection or strain partitioning in this part of the EC (toward the north of 4°N). In this case, our strain data related to convergence of these plates would show only a minor degree of strain deflection or strain partitioning related to intraplate deformation, which is not the case of the present observed deformation in the western border of the northern Andes (westward of the Romeral fault zone).

[35] On the other hand, in our study of deformation patterns in the EC, we gave the name paleostress to finite directions of stress stages deducted from brittle structures. In consequence, a true tectonic sequence of stress in the study area is not carried out because of the lack of evidence on incremental strain stages or additional data concerning rotations around vertical axes. However, partial evidence concerning the relative chronology between different finite stress stages (i.e., field evidence of pre and postfolding structures associated to a particular direction), allows us to propose a possible sequence of stress evolution. Finally, the map scale homogeneity of major directions of the finite stress stages deducted from our analyses, suggests that no large regional rotations seem to have existed around vertical axes in the study area. However, this uncertainty must be tested throughout additional studies, including paleomagnetic data.

3.2. Previous Works

[36] Few paleostress studies have been carried out in the EC. For this reason, the structural reconstructions of the regional structure simply assumed a NW-SE principal direction of shortening, perpendicular to the present-day structural grain of the EC thrust belt [*Colletta et al.*, 1990; *Dengo and Covey*, 1993; *Sarmiento*, 2001]. Previous paleostress descriptions have been made by *Mojica and Scheidegger* [1984] and *Kammer* [1999], delineating compressive trends that vary from NNW to WSW. In the Upper Magdalena Valley (Figure 2), *Cortés* [1994] identified two types of small-scale folds associated with NW-SE and E-W vergences of reverse faulting in Upper Cretaceous rocks, (Olini Group, Figure 6). *Kammer* [1999], on the basis of structural field data and fault patterns, suggested transpression in the EC. *Sarmiento* [2001] suggested transpressional trends based on a map view restoration of the EC. *Montes* [2001] identified an early Paleogene transpressive system in the western flank of the EC south of the Ibague fault, related to ENE-WSW tectonic transport. *Taboada et al.* [2000] reported three tectonic events in the EC. The first event or early Andean phase was identified in rock formations of Mesozoic age with no prevailing trend. The second event, the Andean phase, corresponds to NW-SE contraction in the area of the Sabana de Bogotá and WNW compression in the Guaduas Syncline. This difference was interpreted in terms of rotation of stress and structures of the Guaduas Syncline region with respect to the Sabana de Bogotá. The late Andean phase was identified by *Taboada et al.* [2000] in outcrops of Plio-Quaternary age, showing NW-SE trends of compression in the central part of the EC and high levels of dispersion near the Santa Marta-Bucaramanga wrench fault, which we interpret as a zone of active stress deflection (Figure 2). Because of the large uncertainties that still exist in trends of contraction at different stages of belt evolution, we undertook a compre-

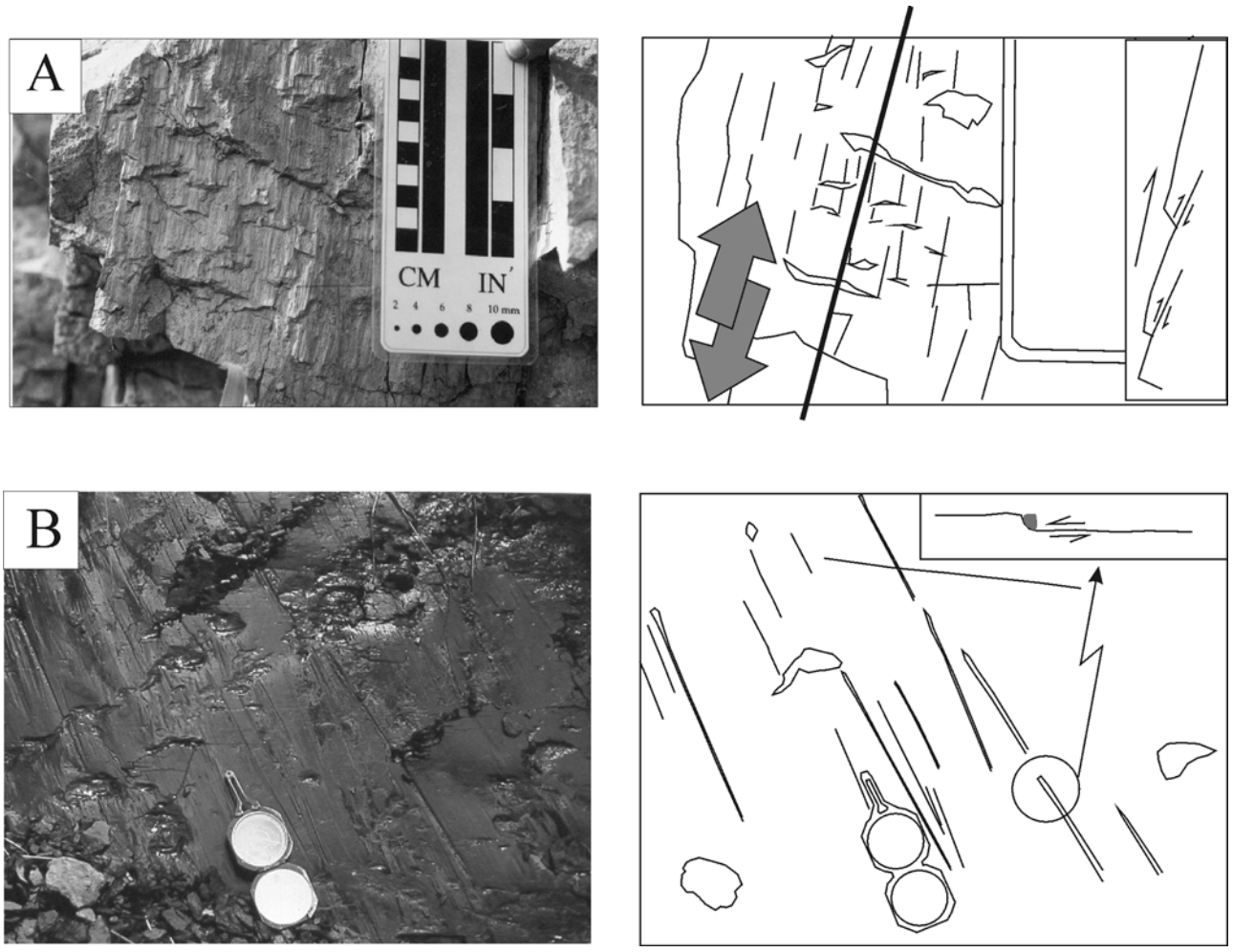

Figure 8. (a) Subvertical minor fault with Riedel's shear structures as criteria to fault sense in fine-grained sandstones. (b) Striations along the fault plane in black shales of the Villeta Group. Note the striate lineation related to the drag of small objects along the fault plane.

hensive paleostress analysis in the Guaduas Syncline and the Sabana de Bogotá areas (Figures 4 and 5); two regions of the EC showing different structural trends.

3.3. Localities

[37] Stress analysis was conducted in the Guaduas Syncline-Apulo region and in the Sabana de Bogotá plateau (Figures 4 and 5). Detailed mapping by using aerial photographs at 1:25,000 scale and radar imagery preceded field mapping. More that 500 field stations were visited, in which available strain markers were collected. All brittle structures were taken into account including stylolites, filled veins, joints, slaty cleavage, and bedding (S0). Some of the most relevant data are presented in Figure 7. However, most of the paleostress determinations were based on the inversion of fault slip data.

3.4. Fault Slip Data

[38] Two main types of fault slip markers were found in the field. The first type corresponds to minor faults in conglomeratic to coarse-grained units with striation and development of Riedel's shears. The second type, in fine-grained rocks (i.e., shales of the Cretaceous Villeta Group), shows lineations related to small striating objects along the fault surface. In both cases, the small structures allow accurate determination of the direction and sense of fault displacement (Figure 8).

[39] Our analysis of fault slip data is based on the inverse method described by *Angelier* [1989, 1990], which allows determinations of the directions of principal stress axes $\sigma1$ (maximum compressive stress), $\sigma2$ (intermediate principal stress) and $\sigma3$ (minimum stress), as well as the ratio of principal stress differences, $\Phi = (\sigma2 - \sigma3)/(\sigma1 - \sigma3)$. Depending on the size of the local fault data sets, we use fault slip data from different outcrops to constrain a single stress direction. In these cases, we combine only data located in the same structure (i.e., Villeta Anticline) and in the same stratigraphic unit. An example of such a combination is presented in Figure 9a, with data from four sites around the axial zone of the Villeta Anticline (Figure 5). Determinations of stress tensor were made at

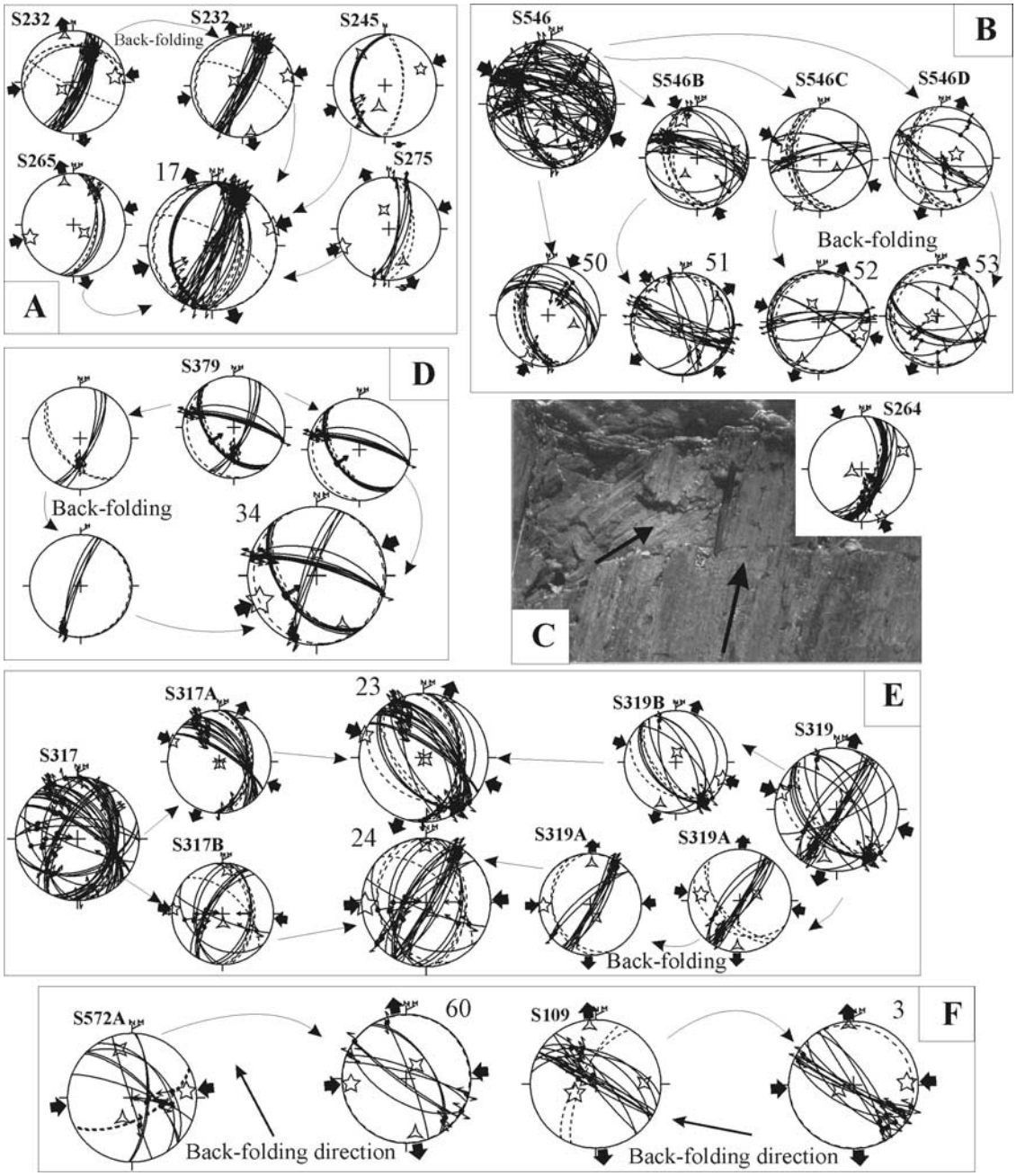

Figure 9. Some examples of paleostress determinations: (a) Determination 17, combination of faults from different sites around the axial zone of the Villeta Anticline to constrain a WSW-ENE contraction. (b) From a single outcrop (S 546) in the Sabana de Bogotá area, selected compatible fault planes allows to the separation of five different stress patterns and unfolding permitted an accurate determination of strain tensors. (c) In the Villeta Anticline area, photograph of minor fault plane presenting two compatible striated patterns, reflecting reactivation of this fault plane coeval with folding. (d) From outcrop S379 in the axial zone of the Villeta Anticline, incompatible fault patterns became compatible after unfolding of inclined shear lineations, evidencing coeval development of faulting and folding. (e) Combination of selected fault surfaces of adjacent sites 317 and 319 allows the determination of WNW-ESE and E-W patterns of faulting, unfolding necessary in E-W contraction post-dates this direction. (f) NW-SE unfolding of inclined stress axes and beds produce WSW-ENE patterns of compression.

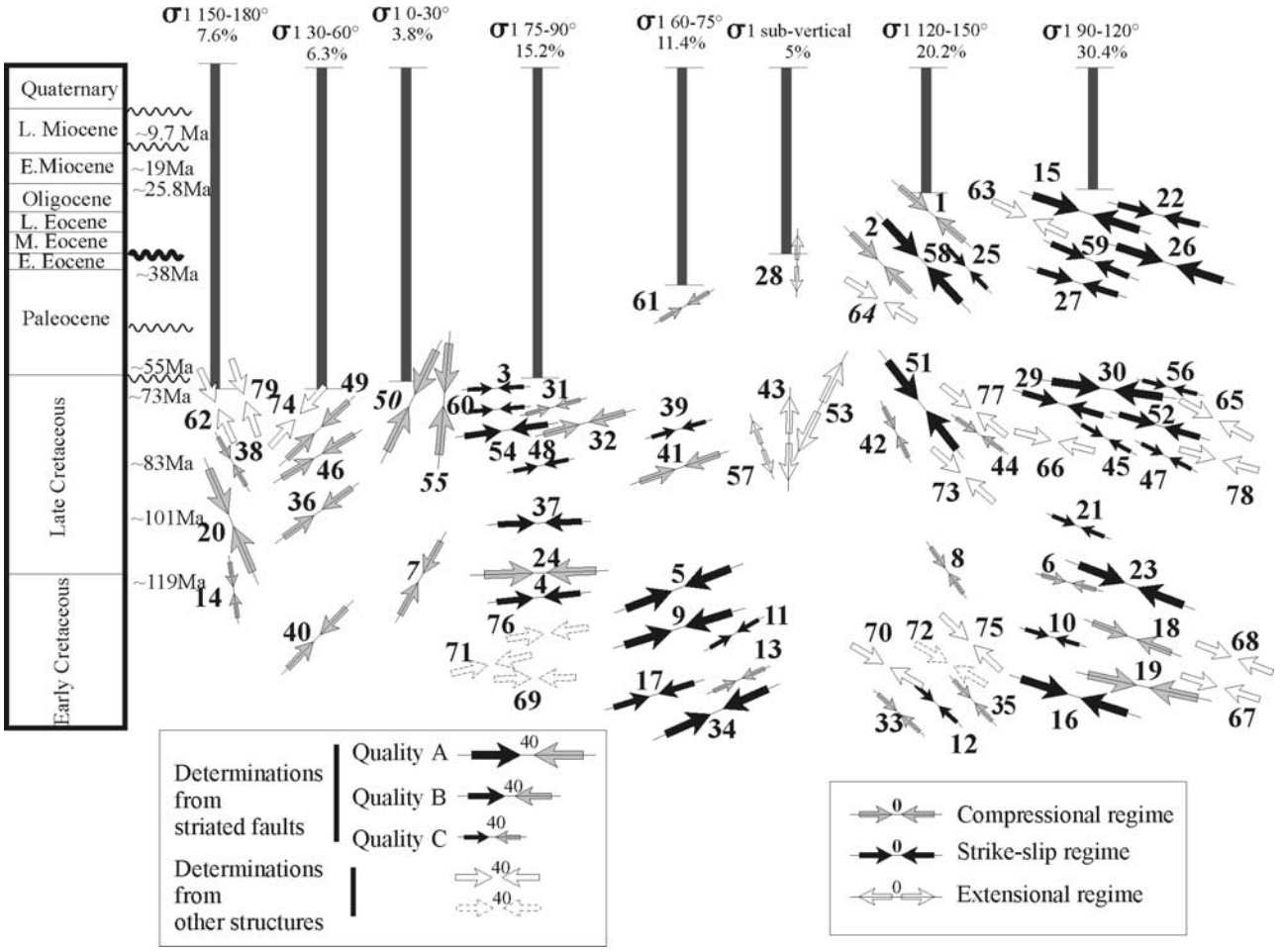

Figure 10. Results of paleostress analysis of this study. In the vertical timescale, each tectonic determination is located in the position of the corresponding outcrop rock. Size of arrows is according to quality factor as in Table 1. Vertical bars indicate the possible age range for the occurrence of each stress regime (youngest to the right). The range of σ1 azimuth defining each stress regime and the percentage of data fitting this range are specified on top of the bars.

each site and often provide similar results, but they were considered less reliable than those of the whole group because of the limited variety in fault orientations.

[40] Superpositions of slickenside lineations were found and reveal polyphase slip, which in several cases reflects polyphase tectonics (especially where different slip patterns are mechanically incompatible). For instance, at sites S546 and 317–319 (Figures 9b and 9e, respectively), we were able to separate different stress regimes in an area where fault reactivation occurred. In other cases, different slips on the same fault surface could be explained with a single stress tensor, suggesting reactivation of the same fault plane coeval with folding during the same tectonic phase (Figure 9c). Note also that folding results in apparent polyphase fault patterns, because of the association of the pretilt, syntilt and posttilt fault slips. Incompatible fault patterns may also become compatible after back-folding, restoring initial attitudes (Figure 9d). Ignoring syntectonic development of faulting and folding during a single major tectonic event may result in overestimation of the number of tectonic regimes.

[41] Our analysis of fault data sets often revealed inclined attitudes of the principal stress axes. In most cases, bedding and axis attitudes are related. Unfolding of data is based on consideration of stratal dip and yields restored principal stress axes that are generally found to be nearly horizontal or vertical. This back-tilting was used as a criterion to determine the relative chronology between different stress patterns as shown in Figure 9f, where it suggests that faults related to E-W contraction were later passively rotated during folding.

3.5. Successive Stress Patterns

[42] Figure 10 illustrates the results of stress analysis in terms of compression trends. Each determination is shown in regard to the age of the stratigraphic unit in which the data were collected. In Table 1, the corresponding numerical values are listed, including the trend and plunge of each principal stress axis as well as the ratio Φ previously defined. Table 1 also includes a general quality estimation of each result. Quality mainly depends on the number of faults and brittle structures measured and on the number of

possible stress regimes. Letters A, B, and C refer to good, average, and poor quality, respectively. No data could be collected in rocks younger than early Oligocene. From Figure 10, two major trends emerge. One trend reveals a contraction pattern changing from E-W to WSW-ENE. The other trend suggests a direction of contraction changing from NW-SE to WNW-ESE. Both trends are represented in the whole sedimentary sequence until the early Eocene.

[43] A critical issue deals with the relative chronology between these -two main patterns, because in most areas of study the same formations are affected. However, NW-SE to WNW-ESE compression was clearly identified with A and B quality determinations in several postearly Eocene outcrops (determinations 15, 22, 58, and 59 of Table 1 and Figures 11a–11b), as well as in structures that cut postlate Miocene structures. Determinations of WSW-ESE and E-W compression were made in rocks of preearly Eocene units. This relative age indication is strengthened by structural evidence. Unfolding in a NW-SE direction of apparently ambiguous data became well-constrained WSW-ENE or E-W stress directions. The unfolding procedure reveals a younger age of the NW-SE and WNW-ESE compression, compared with the E-W and WSW-ENE compression (Figure 9f).

[44] In some cases (e.g., Figures 9e and 9f), folded fault patterns effectively indicate an E-W to WSW contraction, predating NW-SE to WNW compression. This observation is confirmed by strike-slip faults associated to WNW-ESE contraction cutting and offsetting post-Miocene to recent structures in the western flank of the Guaduas Syncline and along the Cambao fault (sites 346, 349, 351, and 365 corresponding to determinations 22, 25, 27 and 29 of list 1 and Figures 7, 8, and 11a–11b).

[45] The relative chronology between the paleostress regimes highlights a regional change in direction of contraction and tendencies of stress patterns in the EC. This change is closely related in time with the late Paleocene-early Eocene regional unconformity of the Magdalena Valley and the western flank of the EC. Accepting the Paleocene age of the Hoyón Formation and its stratigraphic position below this unconformity, we date the most recent good quality data showing WSW-ENE compression as prelate Paleocene (Figure 10). The regional late Paleocene-early Eocene regional unconformity indicates not only strong erosion related to active faulting at this time but also a regional change in stress regime, which is suggested with the temporal distribution of our tectonic determinations in the EC. In addition, the geographic distribution of structures related to each of these major stress directions, also represented on the geological map, shows a rather homogeneous distribution, suggesting that effectively these structures are indeed related to regional independent tectonic phases (Figure 12).

[46] About 18% of our reconstructions could not be classified because their trend of compression was beyond the bounds adopted to define the two main stress patterns. These $\sigma 1$ trends are 0–30 for 3.8% of the data, 150–180 for 7.6% and 130–60 for 6.3% (Figure 10). These amounts were considered too small to permit the identification of additional stress patterns. For determinations 14 and 38 (Figures 10 and 11a–11b; Table 1), the low quality of the reconstructions could explain the ambiguity. In other cases, most data are of good or acceptable B quality. In the Sabana de Bogotá area two sites are close to recent left-lateral strike-slip faults and the SSW-NNE compression is clearly postfolding (sites 523, 546 and 547 Figure 9b and determinations 49, 50 and 55, Figures 7, 11a–11b, and 12; Table 1). This strongly suggests recent local stress deflection around this type of fault. In these cases, local rotation or stress perturbations explain ambiguous trends. Some NNW-SSE and SW-NE compressions certainly exist, but they could be considered as local perturbations of the main NW-SE and WSW-ENE compression respectively. In conclusion, there is no reason to invoke major regional compressions that differ from the two main events discussed in the area and the geological time considered in this paper.

[47] In the Sabana de Bogotá area, some extensional regimes were identified with roughly N-S trending extension, most of them associated to transtension along strike-slip faults (Figure 10 subvertical $\sigma 1$, determinations 43, 53, 57, Figures 7, 11a–11b, and 12; Table 1). All the cases were directly related to salt-doming structures in the Zipaquira area (Figures 7 and 12). Previous works [*Cortés*, 2004; *Montes et al.*, 1994] demonstrated that salt doming structures are related to strike-slip faults in the Sabana de Bogotá. In such models the latter doming event seems to be associated to transtension around these faults with a dominating NW-SE trend and left lateral sense.

[48] The stress regimes inferred from other brittle structures (joints, slaty cleavage and stylolites in Figure 7), are consistent with the directions of contraction indicated by fault-slip data (determinations 62 to 74). Most of these regimes indicate WNW-ESE to NW-SE compression, whereas the WSW-ENE to E-W directions are secondary. This observation suggests that most of the brittle deformation occurred during the Andean tectonic phase. More comprehensive data set collection would be needed to confirm this conclusion.

4. Inferences From Plate Kinematics of the South Caribbean Region

[49] To evaluate the consistency of our model of paleostress derived from field data, we considered the relative movements of plates interacting with the northwestern margin of South America since the Late Cretaceous. Choosing the North America plate as a fixed reference and using published Euler's poles and angular velocities of the South America, Nazca and Caribbean plates (Table 2), we made a backward reconstruction of the relative displacements from the present day to Maastrichtian. Note that the Maastrichtian is the generally accepted time when deformation began in the CC, as well as in the Magdalena Valley and in the EC, in response to the accretion of the WC (see section 1). Through this reconstruction, the directions of convergence between the South America plate and the surrounding plates are calculated and compared with the directions of paleostress derived from our study of inversion of field data in the EC of Colombia (see discussion in section 3.1).

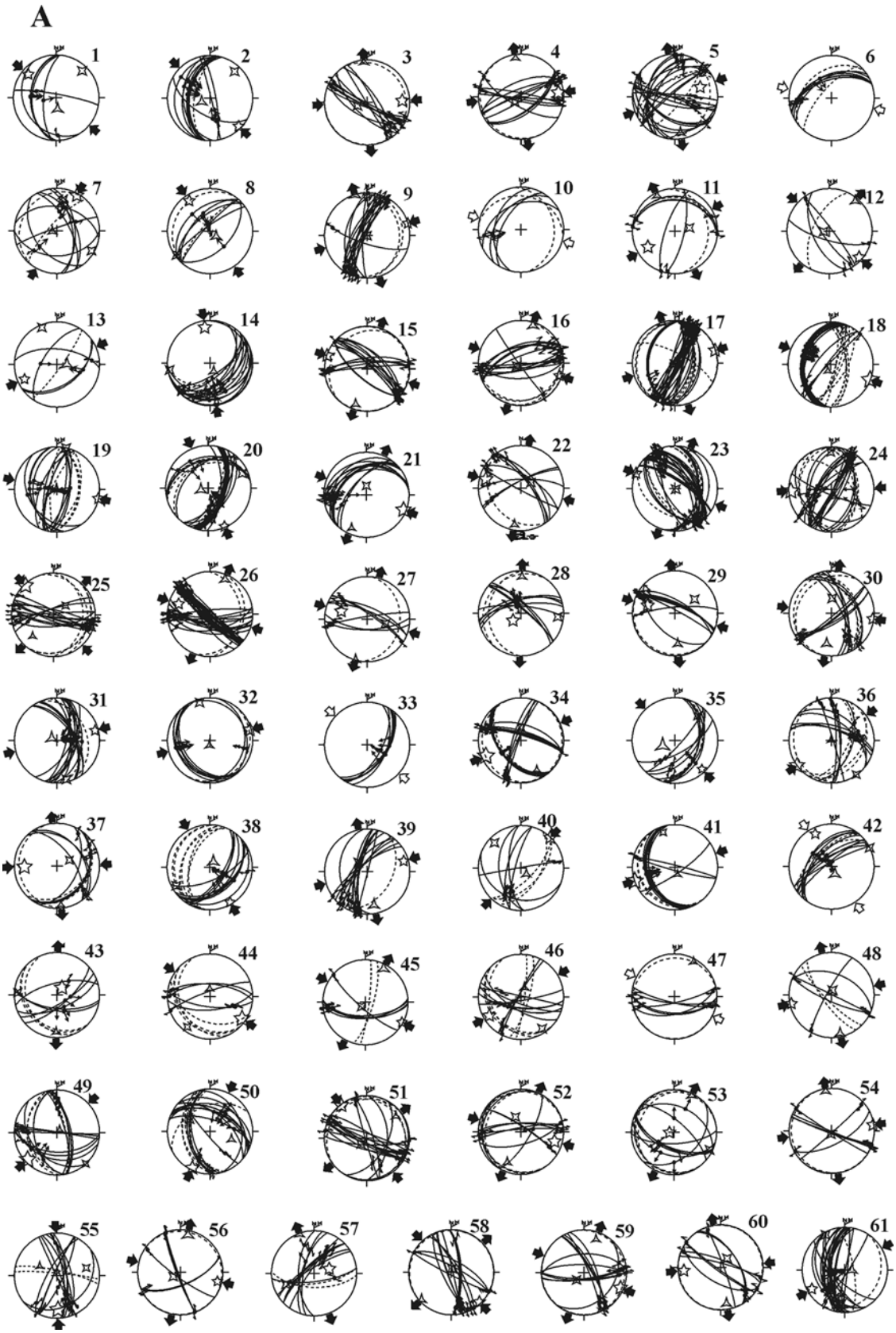
A
1
2
3
4
5
6
7
8
9
10
11
12
13
14
15
16
17
18
19
20
21
22
23
24
25
26
27
28
29
30
31
32
33
34
35
36
37
38
39
40
41
42
43
44
45
46
47
48
49
50
51
52
53
54
55
56
57
58
59
60
61

Figure 11

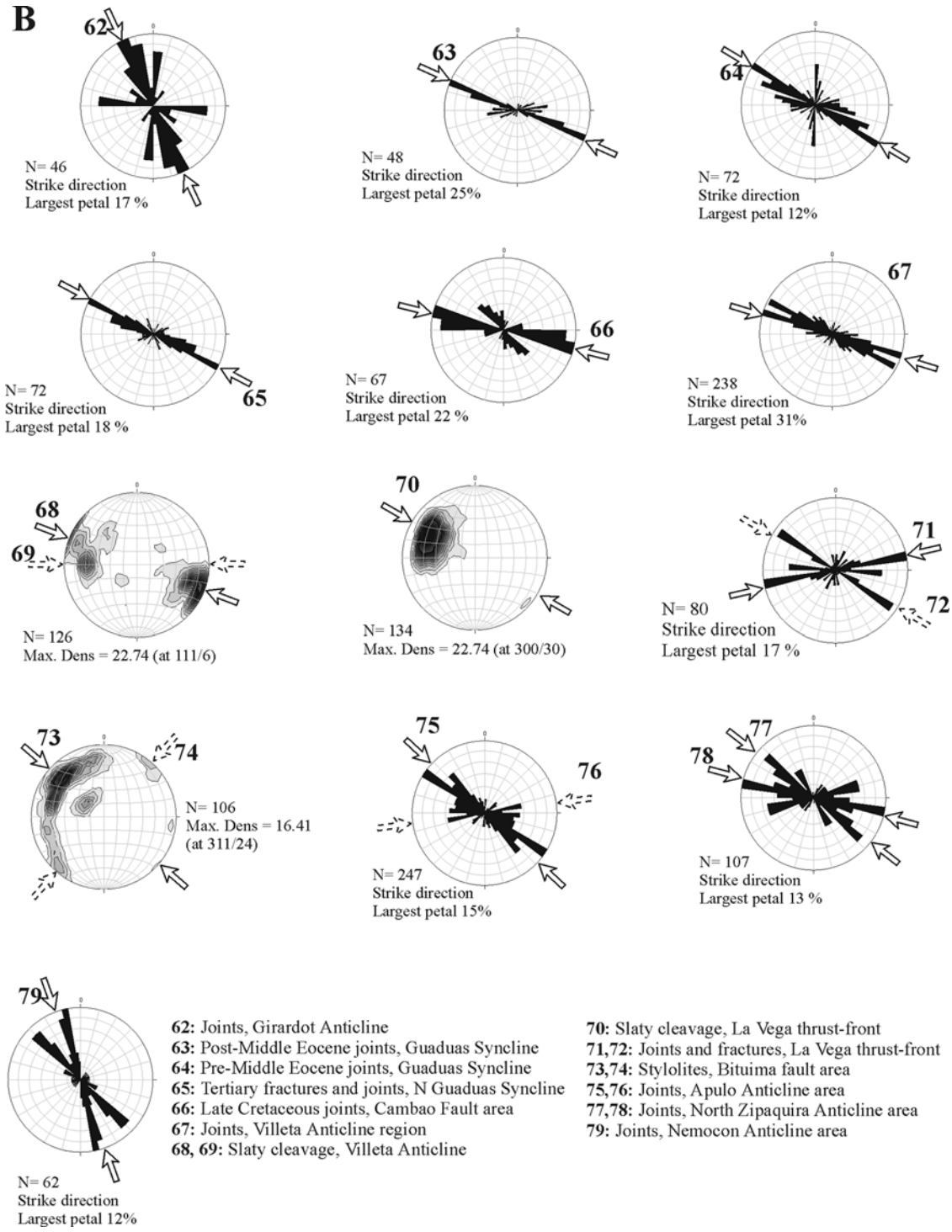

Figure 11. (a) Structural diagrams of paleostress determinations based on fault slip data (lower hemisphere projections). Numbers correspond to stress determination as in Table 1 and arrows in Figures 7, 9, 10, and 12. Dashed lines are bedding (S0) projections. (b) Structural diagrams of inferred paleostress determinations based on kinematic indicators including fractures, joints, slaty cleavage, and stylolites.

[50] The model was built in two main steps. First, we derived the present-day state of contraction in the northern Andes and assumed that this was been constant during the last 9.7 Ma. Second, we calculated the directions of contraction in the NW extreme of the South America plate with the surrounding plates since Late Maastrichtian to 9.7 Ma. In general, we assumed a constant velocity of the Caribbean plate since Maastrichtian, which we estimated

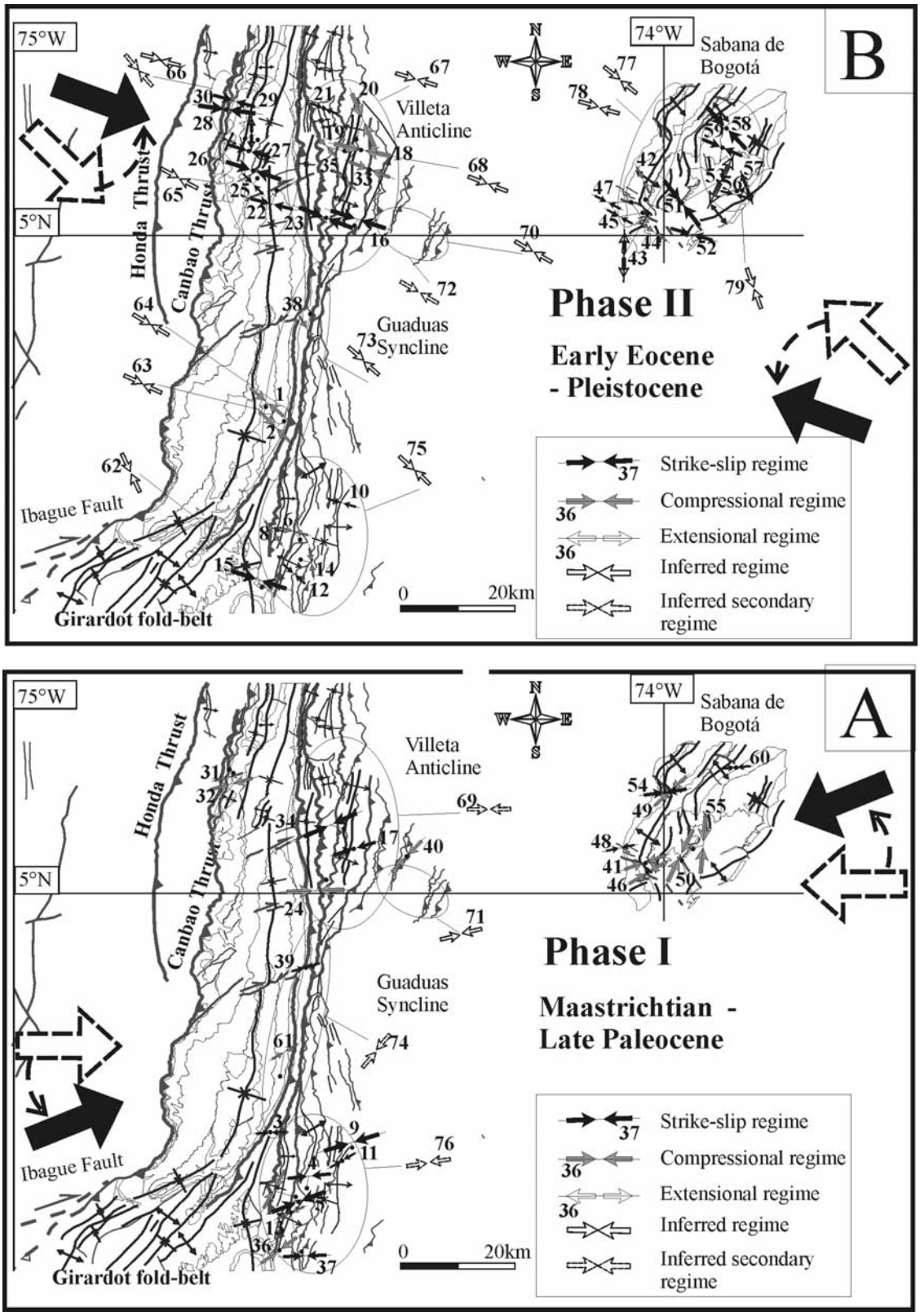

Figure 12. Geological map showing the spatial distribution of structures related to major tectonic phases in the Eastern Cordillera. (a) Pre-Eocene phase associated to E-W to WSW-ENE direction of compression; (b) Postearly Eocene phase associated to NW-SE to WNW-ESE direction of compression.

Table 2. Numerical Values of Euler's Poles and GPS Data Used in the Kinematic Model of Figures 13 and 14[a]

			Pole			
Plate Pairs	Chron.	Age, Ma	Latitude (N+)	Longitude (+E)	Angle, deg	Ref.
SA-NA	0-5	9.7	15.06	−56.59	1.408	1
SA-NA	5-6	19	14.42	−49.56	2.030	1
SA-NA	6-8	25.8	23.08	−55.54	1.727	1
SA-NA	8-18	38.4	20.57	−58.63	1.358	1
SA-NA	18-25	55.9	1.76	−49.85	2.355	1
SA-NA	25-30	65.6	−43.69	−80.57	0.488	1
SA-NA	30-33	73.6	−31.75	−124.85	0.557	1
SA-NA	33-34	83	−32.74	−102.67	0.417	1
CA-NA	0-5	9.7	−30.1	−71.4	2.045	2
CA-NA	5-6	19	−30.1	−71.4	1.959	2
CA-NA	6-8	25.8	−30.1	−71.4	1.432	2
CA-NA	8-18	38.4	−30.1	−71.4	2.654	2
CA-NA	18-25	55.9	−30.1	−71.4	3.685	2
CA-NA	25-30	65.6	−30.1	−71.4	2.043	2
CA-NA	30-33	73.6	−30.1	−71.4	1.685	2
CA-NA	33-34	83	−30.1	−71.4	1.982	2
CA-SA	PD	PD	50	−65.3	2.045[b]	3
CA-SA	PD	PD	68.4	−126.3	2.045[b]	3
			GPS Data			
Plate	Site[c]	Chron.	North, mm/year	East, mm/year		Ref.
NAZ	MALS	PD	53.62	1.43		4
CAR	SANA	PD	19.18	−4.49		4
PCB	CHIT	PD	30.48	0.69		4
NAN	BOG	PD	5.78	1.29		4
SA	VILL	PD	0.00	−2.53		4

[a]References are numbered as follows: 1, *Müller et al.* [1999]; 2, *DeMets et al.* [1990]; 3, *Deng and Sykes* [1995]; 4, *Freymueller et al.* [1993]. The first plate moves counterclockwise relative to the second plate. Abbreviations are as follows: SA, South American plate; NA, North American plate; CA, Caribbean plate; NAZ, Nazca plate; PCB, Panama-Choco Block; NAN, North Andes Block; PD, present day.
[b]Velocity from this study.
[c]Sites chosen for present-day model of Figures 11a–11b [*Freymueller et al.*, 1993].

around 0.21°/Myr. We explain the model in detail in the next sections.

4.1. Present-Day Kinematics

[51] As previously mentioned, the present deformation in the northern Andes results from interaction of NW South America with the Nazca and Caribbean plates, and the Panama-Choco Block (PCB) (Figure 13). We consider the relative direction of convergence between the major plates and the block displacements relative to North America since 9.7 Ma, which roughly coincides in time with the onset of the collision between the PCB, and the northern Andes.

[52] Because of the previously discussed nature and tectonic complexity of the Caribbean plate, a variety of Euler's poles have been proposed to describe its displacement [*DeMets*, 1993; *DeMets et al.*, 1990; *Deng and Sykes*, 1995; *Dixon et al.*, 1998; *Minster and Jordan*, 1978]. We use the poles from *DeMets et al.* [1990] and *Deng and Sykes* [1995] to estimate the relative displacement between the Caribbean and South America plates during the last 9.7 Ma. The results obtained from these two solutions are compared in Figure 13. We finally compare these results with both the GPS data of *Trenkamp et al.* [2002] and our determination of the latest stress regime affecting the EC as indicated by our tectonic study (see discussion in section 3.1) and we conclude that the Euler pole of the NUVEL-1 model [*DeMets et al.*, 1990] best describes the present-day direction of convergence CA-SA relative to NA. The pole of *Deng and Sykes* [1995] seems appropriate to describe the present-day deformation of the northern and northeastern tips of the Caribbean plate, as noted by *DeMets et al.* [2000]. However, to the south it is not entirely satisfactory as suggested by both GPS data of *Trenkamp et al.* [2002] and our field data. This discrepancy may be related to a nonrigid behavior of the Caribbean plate, which could be experiencing internal deformation as pointed out by *Mauffret and Leroy* [1999].

[53] The data from *Trenkamp et al.* [2002] allow us to incorporate the present-day movement of the North Andes Block and PCB in the kinematic reconstruction. We made this analysis to better constrain the reconstruction previous to 9.7 Ma, assuming that in those times the area of our study behaved as part of the South American plate and not as the North Andes Block. The GPS data show that relative to the North Andes Block, both the Nazca plate and the PCB converge in a roughly E-W direction, whereas the Caribbean plate moves in a WNW-ESE direction relative to the North Andes Block and South America. The pole of *DeMets et al.* [1990] is in agreement with the WNW-ESE direction of convergence between the Caribbean and South American plates. The pole of *Deng and Sykes* [1995] predicted a relative WSW-ENE direction of convergence between

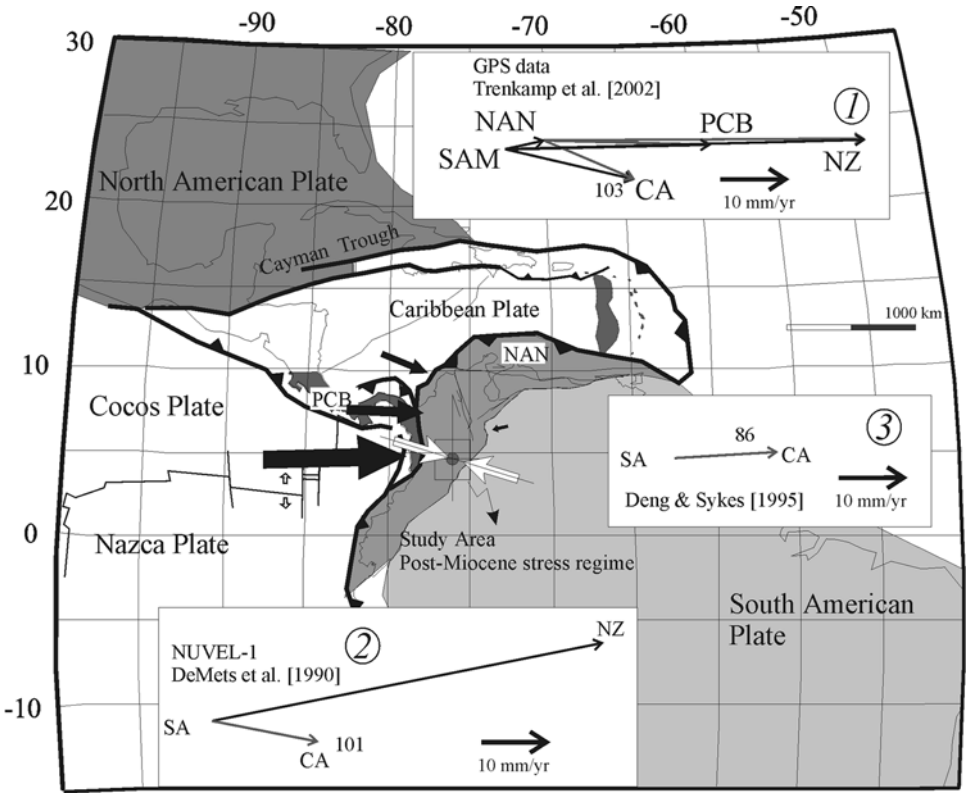

Figure 13. Present-day state of stress in the northern Andes region as deducted from (1) GPS data of *Trenkamp et al.* [2002] (also shown in bold arrows), (2) NUVEL-1 model relative direction of convergence between South America–Caribbean plates and the South America–Nazca plates, and (3) direction of convergence between South America–Caribbean plates according to Euler's pole of *Deng and Sykes* [1995]. Open arrows correspond to present-day stress regime in the study area deducted from field tectonic data. Note that present-day stress in the northern Andes deducted from field data of this study, agree the present direction of convergence between the plates South America–Caribbean derived from pole of NUVEL-1 model.

these plates, which is not consistent with the GPS data (Figure 13). On the other hand, our model based on inversion of field data shows that the post late Miocene faults were related to a WNW-ESE regime with an average N107°E direction of compression.

[54] The GPS data show approximate direction N93°E for convergence between the PCB and the North Andes Block, N112°E for convergence between the CA and the North Andes Block, and N103°E for CA-SA plates convergence, which means, for our model, differences in trend of 14°, 5°, and 4°, respectively. These differences may be interpreted in several ways. The E-W CPB convergence with the North Andes Block may be younger than the Andean WNW-ESE convergence. It is also possible that important stress deflection is occurring in the frontier area of the PCB and the North Andes Block. The minor difference between our results in terms of tectonic compression and the direction of convergence between the South America - Caribbean plates, allows us to estimate that we are in an average error of ±4° when we consider our study area as part of the South American plate. In the EC, we mainly recorded deformation related to South America - Caribbean interaction. Additional work including paleomagnetic determinations in order to identify possible block rotations in the North Andes Block area, in conjunction with inversion of focal mechanisms of earthquakes, would be useful to improve GPS and field tectonic studies.

[55] The Nazca plate was considered as an active part of the reconstruction only since 9.7 Ma to present, when this plate began to interact with the southwestern extreme of the North Andes Block. In order to evaluate the possible effects of the Nazca plate in the area of our study, we used the pole of the NUVEL-1 model [*DeMets et al.*, 1990] for this plate relative to South America and geodetic (GPS) data from *Trenkamp et al.* [2002]. This evaluation showed that neither the E-W nor WSW-ENE directions of convergence between the Nazca plate and the North Andes Block, predicted by the GPS measurements and the NUVEL-1 model respectively, are presently active as E-W or WSW-ENE deformation in the EC, at least north of 4°N (Figure 13).

4.2. Plate Kinematics Reconstruction From Early Coniacian to Late Miocene

[56] In order to estimate directions of contraction in northwestern South America before 9.7 Ma, we restrict the problem to interaction between the South America and

Caribbean plates. This simplification is licit because, as previously discussed, the domain of study roughly behaves as the South America plate. Choosing the NA plate as a fixed reference, we determined the displacement of the South America and Caribbean plates and we derived the predicted paleostress at each step of the reconstruction, assuming parallelism between plate convergence vectors and maximum stress compression in the most internal part of the northern Andes (see discussion in section 3.1). Our kinematic model is shown in nine steps (Figure 14), in agreement with the poles of rotation for the relative movement of the Americas as published by *Müller et al.* [1999]. The numerical values used in the kinematic model are indicated in Table 2.

[57] The trajectory of the Caribbean plate previous to 9.7 Ma is highly speculative for the reasons previously discussed in section 1.1. Indirect evidence has been used to describe the displacement of this plate since the Early Coniacian times, when it became an independent plate. *Pindell and Barret* [1990] simplified the problem and proposed that a pole close to Santiago de Chile in South America could account for eastward displacement of the CP relative to the Americas since Eocene times. Other works agree with this possible location of the pole [*DeMets et al.*, 1990; *Minster and Jordan*, 1978]. Before Eocene time, the models describing paths of the CP agree with a NE displacement of this plate being inserted between the Americas. Because of uncertainties concerning to poles of the CP, and taking into account the very good fit between directions for the last 9,7 Ma derived from the model by using the NUVEL-1 pole [*DeMets et al.*, 1990], we tried to simplify the reconstruction by using this pole from Early Coniacian to present. As a result, the eastward displacement of the Caribbean plate with respect to the Americas was achieved and the NE displacement from Coniacian to Eocene was maintained.

[58] In order to estimate the angular velocity of the Caribbean plate during each phase of the model, we considered the paleogeographic reconstructions of the Early Coniacian concerning the position of Aves ridge as the northern prolongation of the CC [*Mann*, 1999; *Pindell and Barret*, 1990; *Villamil and Pindell*, 1998] and calculated, using the NUVEL-1 pole, its angular distance with respect to its present position in about 17.5° (Figure 14a). Assuming a constant velocity of the CP, we estimated the angular velocity ω in 0.21°/Myr, which is approximately in agreement with the GPS estimations of present-day velocities of the CP relative to NA of 0.19 My^{-1} according to *DeMets et al.* [2000] and 0.25°/Myr according to *Dixon et al.* [1998].

[59] The relative movement of the Americas could be summarized as relative NW-SE divergence since 190 Ma, changing to convergence since about 38.4 Ma ago. According to *Müller et al.* [1999], relative acceleration of convergence during Miocene times caused the activation of underthrusting of the CP below the South America plate and deformation at the interior of the Caribbean plate. In agreement with the conclusions of part 3, the change of the regional pattern of stress in the area of the EC could be related to the relatively accelerated shifting from divergence to convergence of the Americas during the late Paleocene times, producing development of large unconformities in the area of the Magdalena Valley and EC and changing the sedimentological regimes and basin mechanisms at that time.

[60] In our kinematic model, we have used the approximate reconstructed geometry of the continental border of northwestern South America as presented by *Pindell and Barret* [1990], *Mann* [1999], and *Villamil and Pindell* [1998], in order to maintain the frontier conditions at the moment of each tectonic event. We also introduced in the model the present geographic north and we rotated it with the South American plate as a reference to compare the trend of paleostress.

[61] The kinematic model could be summarized as a general E-W to WSW-ENE convergence of the WC with the western border of South America during the Early Maastrichtian to late Paleocene (Figures 14a–14d). This paleostress resulted from the combined effect of relative divergence of the Americas and SW-NE convergence of the South America-Caribbean plates. Obliquity of the strain regime relative to faults in the east border of the NA block and the Jurassic normal faults bounding the basin of the EC (e.g., Guaicaramo and Ibague faults, Figures 2 and 5), provides the necessary conditions for right lateral strike-slip displacement of these faults in the EC and Magdalena Valley from Early Maastrichtian to late Paleocene. Evidence of pre-Eocene positive flower structures has been reported in the Middle Magdalena Valley by *Suarez et al.* [2000] and *Pindell et al.* [1998] and active transpression at that time was demonstrated by *Montes* [2001] in the western flank of the EC.

[62] Since the middle Eocene (~38.4 Ma.) a new NW-SE compressive stress regime was dominant and lasted until postlate Miocene times when compression became WNW-ESE. This regime resulted mainly in the change from relative divergence to convergence between the Americas at the end of the Paleocene, accompanied by an eastward displacement of the Caribbean plate relative to the Americas (Figures 14e–14i).

[63] In Figure 15, the results of paleostress determinations from field tectonic data are compared with convergence directions predicted from the kinematic model of the Southern Caribbean. From Figure 15 we can conclude that our model of stress evolution in the northern Andes is consistent and could be explained in terms of regional contraction of the northwestern margin of South America as it interacted with the Caribbean plate since Late Cretaceous times. An important change in stress regimes at the end of the Paleocene is observed both in the theoretical kinematic model and the observed field data.

5. Discussion and Conclusions

[64] Our inversion of tectonic data revealed two main trends of compressive paleostress in the Eastern Cordillera of Colombia and their chronology was established based on both stratigraphic and tectonic relative chronology criteria.

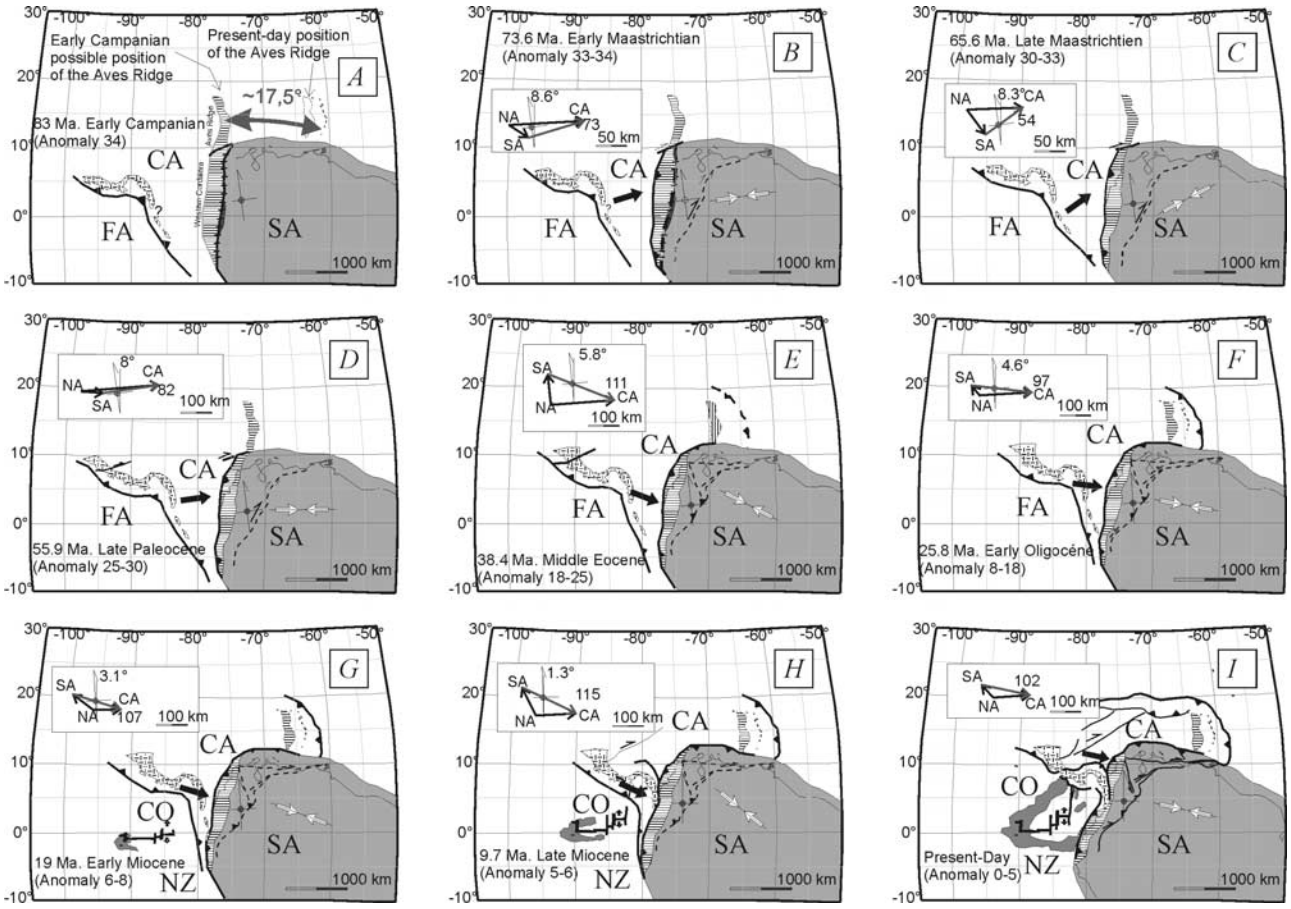

Figure 14. Simplified kinematic model of the South Caribbean region used to calculate directions of convergence of the South America–Caribbean plates. Kinematic solutions presented as triangles in each step including the regional trend of the Caribbean–South America convergence, presented also as bold arrows, and paleonorth deviation with respect to present magnetic north. White arrows indicate the directions of plate convergence corrected with respect to present-day magnetic north. In Figure 14a, an angular distance of 17.5° (centered in the Euler's pole of NUVEL-1 model) was assumed for position of the Aves Ridge during the Early Coniacian [after *Pindell and Barret*, 1990], relative to its present-day position. Figures 14a–14d show an E-W to WSW-ENE convergence, inducing right lateral shear in ancient normal faults. During late Paleocene to present-day (Figures 14e–14i), a regional change to NW-SW convergence induces basin inversion and fold-and-thrust belt development. In the last 9.7 Ma (Figure 14i) the regional regime became WNW-ESE during the Andean tectonic phase. Abbreviations are as follows: FA, Farallon plate; CA, Caribbean plate; SA, South American plate; CO, Cocos plate; NZ, Nazca plate.

E-W to WSW-ENE direction of contraction was not identified in rocks younger than early Eocene, suggesting a late Paleocene to early Eocene age for this stress regime. The second stress regime reveals a NW-SE to WNW-ESE direction of compression; this regime was recorded in rocks as old as Oligocene. This second major compression was also characterized along post-Miocene and Quaternary structures such as the Guaduas Syncline and structures affecting the Guaduas Syncline, allowing relative dating of this regime as the most recent one. It is worth noting, however, that in detail the tectonic history may involve more than two regimes, so that the two-step history defined above should be regarded as a first-order approximation. Identifying second-order events would require a large mass of data and stratigraphic datings, which was not available in the study area.

[65] This major change in the regional stress directions coincides with the time of development of a regional unconformity in Colombia, traditionally referred to as the middle Eocene Unconformity. This unconformity is characterized by large angles in the western flank of the Eastern Cordillera and the Magdalena Valley. We infer that the change in the regional stress pattern corresponds to a major change in the regional structural style.

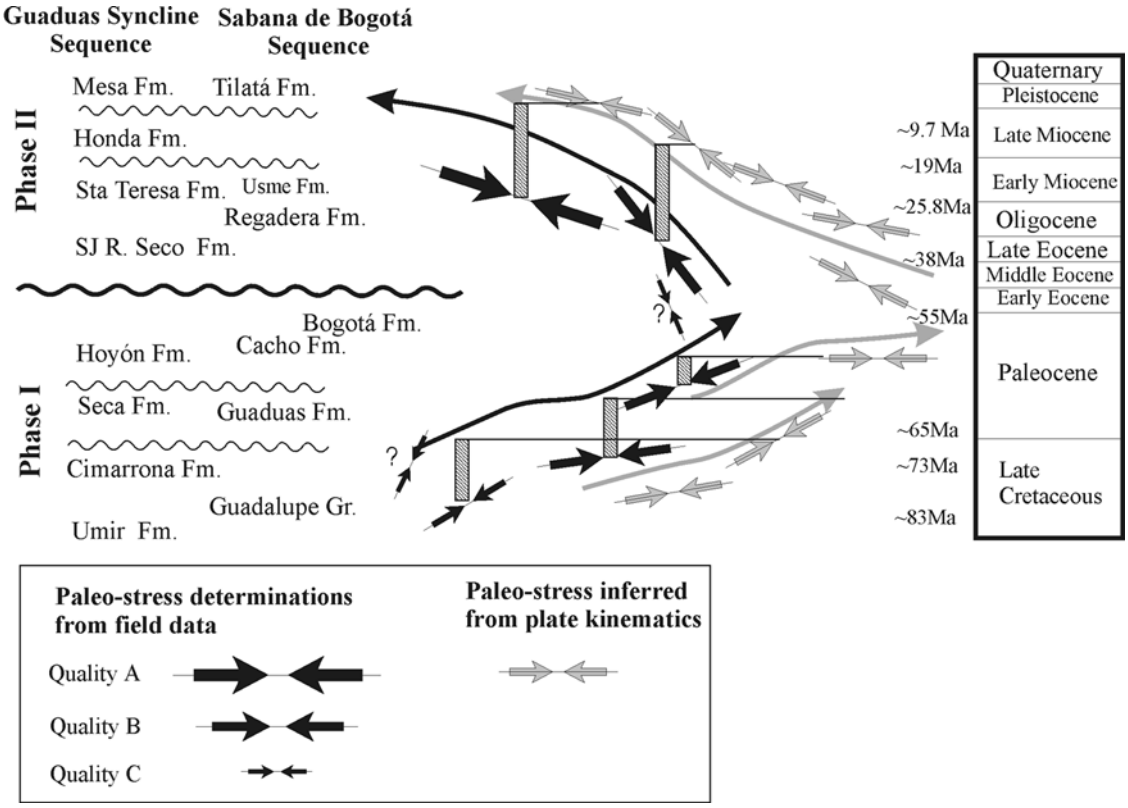

Figure 15. Interpretation of paleostress determinations from analyses of field tectonic data (bold arrows on the left), and paleostress predicted from the kinematic model of plates (gray arrows on the right including north correction). In both cases an E-W to WSW-ENE contraction precedes a change in the regional pattern of stress at the end of the Paleocene, followed by a NW-SE direction of contraction that rotates to WNW-ESE during the late Miocene. The size of bold arrows for the field data is in accordance with the number of determinations constraining the average direction of contraction. Vertical bars show the possible rock sequence affected by the stress regime indicated on top of each bar with a horizontal line.

[66] A kinematic model of the southern Caribbean region was built in order to explain our sequence of stress evolution in terms of interaction between the northwestern corner of the South American plate and the surrounding plates since the Maastrichtian times. We used the NA plate as a fixed reference, and we adopted published poles of the South America and Caribbean plates to derive directions of convergence of these plates. We also assumed rough parallelisms between the paleostress compressional trends and the convergence directions, knowing that this is an approximation. A critical point was the definition of the Euler's pole to be used for the Caribbean plate, given the variety of poles available for this plate in the literature. We found that the pole issued from the NUVEL -1 model [*DeMets et al.*, 1990] best described both the present-day deformation patterns and the GPS geodetic data in the southern Caribbean area and hence was adopted in our model.

[67] A good fit was achieved between the model based on inversion of field data and that issued from plate kinematics. Both these models predict an E-W to WSW-ENE pattern of contraction or plate convergence until the late Paleocene, followed by a change in these directions to NW-SE to WNW-ESE from the late Paleocene to the present day. In the kinematic model, the change from relative divergence to convergence between the Americas induced a change in regional directions of convergence of the Caribbean- South America plates. We thus propose that this kinematic change to convergence between the Americas during the late Paleocene to early Eocene times, was responsible for the main change in stress patterns and structural style that we independently reconstructed in the northern Andes. Furthermore, this major change was recorded in the study area as a pronounced angular unconformity that separates two well-defined structural styles.

[68] Positive flower structures below the late Paleocene-early Eocene unconformity in the Magdalena Valley are commonly identified based on seismic reflection profiles. On the other hand, the post-Eocene structures are characterized by inversion of ancient NE-SW trending normal faults accompanied by development of fold-and-thrust belts. These observations are consistent with the sequence of stress patterns defined above, considering that an E-W to WSW-ENE principal direction of contraction applied to NE-SW ancient normal faults should produce

dextral strike-slip displacement along these structures and the NW-SE to WNW-ESE direction of contraction is quite appropriate to produce tectonic inversion along them.

[69] Our fault kinematic data revealing the present-day stress regime dominated by WNW-ESE compression are quite compatible with the general direction of the present-day convergence between the South American and Caribbean plates. This agreement brings confirmation to previous conclusions about an marked geodynamic influence of the Caribbean plate in the northern segment of the northern Andes [*Ego et al.*, 1996]. It also implies that a compressive present-day regime prevails along the major ENE-WSE trending faults that bound the Eastern Cordillera. This pattern argues against simple models based on GPS data suggesting that the northern Andes is a mobile block escaping toward the ENE, implying a transpressive stress regime in the eastern margin of the Eastern Cordillera. Our field data concerning fault mechanisms and kinematics rather suggest a dominant compressive behavior of the eastern margin, which supports the results of previous works based on analyses of field data, focal mechanisms of earthquakes and balanced cross sections [*Branquet et al.*, 2002; *Casero et al.*, 1997; *Colletta et al.*, 1990; *Corredor*, 2003; *Cortés*, 2004; *Dimate et al.*, 2003; *Rowan and Linares*, 2000; *Taboada et al.*, 2000]. Our results also suggest that the northern Andes should be considered as accommodating deformation in a complex manner, under at least two distinct stress regimes (E-W Nazca-related regime, and WNW-ESE Caribbean-related one), rather than being a single escaping mobile block as suggested by GPS data. The interpretation of kinematics and seismotectonic stress data deserves caution in such a complex tectonic area where most present-day data merely represent local strain associated to an interseismic period.

[70] **Acknowledgments.** This study was supported by the Fundación COLFUTURO (Bogotá), the Fundación Para la Promoción de la Ciencia y la Tecnología-Banco de la República, research project 1102 (Bogotá), the Corporación Geológica Ares (Bogotá) and EGID (Paris). We are grateful to Claudia Osorio and Germán Bayona for discussion and comments on the manuscript and Fabricio Cómbita for assistance in the field. We thank Alfredo Taboada and Luis Fernando Sarmiento for critical and constructive comments that greatly improved the original manuscript.

References

Alvarez, A. J. (1983), Geología de la Cordillera Central y el occidente Colombiano y petroquímica de los intrusivos granitoides mesocenozoicos, *Bol. Geol. Ingeominas*, *26*, 175 pp.

Alvarez, E., and H. Gonzalez (1978), Geología del Cuadrángulo I-7 Urrao, scale 1:100,000, Ingeominas, Medellin, Colombia.

Amezquita, F., and C. Montes (1994), Sección Geológica El Maco-Buenavista: Estructura en el sector occidental del Valle Superior del Magdalena, in *Estudios Geológicos del Valle Superior del Magdalena*, vol. VI, 36 pp., Univ. Nacl. de Colombia-Ecopetrol, Bogotá.

Angelier, J. (1989), From orientation to magnitudes in paleostress determinations using fault slip data, *J. Struct. Geol.*, *11*, 37–50.

Angelier, J. (1990), Inversion of field data in fault tectonics to obtain the regional stress, III, A new rapid direct inversion method by analytical means, *Geophys. J. Int.*, *103*, 363–376.

Barrero, D. (1979), Geology of the central Western Cordillera, west of Buga and Roldanillo Colombia, *Publ. Geol. Espec. Ingeominas*, *4*, 75 pp.

Bourgois, J., B. Calle, J. Tournon, and J. F. Toussaint (1982), The Andean ophiolitic megastructures on the Buga-Buenaventura transverse (Western Cordillera -Valle Colombia), *Tectonophysics*, *82*, 207–229.

Bourgois, J., J. F. Toussaint, H. Gonzalez, J. Azema, B. Calle, A. Desmet, L. A. Murcia, A. P. Acevedo, E. Parra, and J. Tournon (1987), Geological history of the Cretaceous ophiolitic complex of northwestern South America (Colombian Andes), *Tectonophysics*, *143*, 307–327.

Branquet, Y., A. Cheilletz, P. R. Cobbold, P. Baby, B. Laumonier, and G. Giuliani (2002), Andean deformation and rift inversion, eastern edge of Cordillera Oriental (Guateque-Medina area), Colombia, *J. S. Am. Earth Sci.*, *15*, 391–407.

Burke, K., P. J. Fox, and A. M. C. Sengor (1978), Buoyant ocean floor and the evolution of the Caribbean, *J. Geophys. Res.*, *83*, 3949–3954.

Burke, K., C. Cooper, J. F. Dewey, P. Mann, and J. L. Pindell (1984), Caribbean tectonics and relative plate motions, *Mem. Geol. Soc. Am.*, *162*, 31–63.

Cáceres, C., and F. Etayo-Serna (1969), Bosquejo geológico de la región del Tequendama: Opúsculo guía de la excursión pre-congreso, paper presented at I Congreso Colombiano de Geología, Fac. de Cienc., Univ. Nacl. de Colombia, Bogotá.

Cáceres, C., F. Etayo-Serna, R. Llinás, M. Rubiano, and L. Pérez (1970), Mapa geológico del Cuadrángulo L-10, Fusagasugá, scale 1:100,000, Ingeominas, Bogotá.

Case, J. E., S. L. Durán, R. A. Lopez, and W. R. Moore (1971), Tectonic investigations in western Colombia and eastern Panama, *Geol. Soc. Am. Bull.*, *82*, 2685–2712.

Case, J. E., J. Barnes, Q. Paris, I. H. Gonzalez, and A. Viña (1973), Trans-Andean geophysical profile, southern Colombia, *Geol. Soc. Am. Bull.*, *84*, 2895–2904.

Casero, P., J. F. Salel, and A. Rossato (1997), Multidisciplinary correlative evidences for polyphase geological evolution of the foot-hills of the Cordillera Oriental (Colombia), paper presented at VI Simposio Bolivariano de Exploracion Petrolera en las Cuencas Subanadinas, Asoc. Colombiana de Geol. y Geofis. del Petrol., Cartagena, Colombia.

Cediel, F., and C. Cáceres (1988), Geologic map of Colombia, scale 1:1,200,000, Geotec, Bogotá.

Colletta, B., F. Hebrard, J. Letouzey, P. Werner, and J. L. Rudkiewicz (1990), Tectonic style and crustal structure of the Eastern Cordillera (Colombia) from a balanced cross section, in *Petroleum and Tectonics in Mobile Belts*, edited by J. Letouzey, pp. 81–100, Ed. Technip, Paris.

Cooper, M. A., et al. (1995), Basin development and tectonic history of the Llanos Basin, Eastern Cordillera, and Middle Magdalena Valley, Colombia, *AAPG Bull.*, *79*, 1421–1443.

Corredor, F. (2003), Seismic strain rates and distributed continental deformation in the northern Andes and three-dimensional seismotectonics of the northwestern South America, *Tectonophysics*, *372*, 147–166.

Cortés, M. (1994), Análisis de la deformación estructural del Grupo Olini en el Valle Superior del Magdalena, in *Estudios Geológicos del Valle Superior del Magdalena*, vol. IX, 16 pp., Univ. Nacl. de Colombia, Ecopetrol, Bogotá.

Cortés, M. (2004), Evolution structurale du Front Centre-Occidental de la Cordillère Orientale de Colombie, Ph.D. thesis, 331 pp., Univ. Pierre et Marie Curie, Paris.

DeMets, C. (1993), Earthquake slip vectors and estimations of present-day plate motions, *J. Geophys. Res.*, *98*, 6703–6714.

DeMets, C., R. G. Gordon, D. F. Argus, and S. Stein (1990), Current plate motions, *Geophys. J. Int.*, *101*, 425–478.

DeMets, C., P. Jansma, G. S. Mattioli, T. H. Dixon, F. Farina, R. Bilham, E. Calais, and P. Mann (2000), GPS geodetic constrains on Caribbean-North America plate motion, *Geophys. Res. Lett.*, *27*, 437–440.

Deng, J., and L. R. Sykes (1995), Determination of Euler pole for contemporary relative motion of Caribbean and North American plates using slip vectors of interplate earthquakes, *Tectonics*, *14*, 39–53.

Dengo, C. A., and M. C. Covey (1993), Structure of the Eastern Cordillera of Colombia: Implications for trap styles and regional tectonics, *AAPG Bull.*, *77*, 1315–1337.

Dewey, J. W. (1972), Seismicity and tectonics of western Venezuela, *Bull. Seismol. Soc. Am.*, *62*, 1711–1751.

Dimate, C., L. Rivera, A. Taboada, D. Bertrand, A. Osorio, E. Jimenez, A. Fuenzalida, A. Cisternas, and I. Gomez (2003), The 19 January 1995 Tauramena (Colombia) earthquake: Geometry and stress regime, *Tectonophysics*, *363*, 159–180.

Dixon, T. H., F. Farina, C. DeMets, P. Jansma, P. Mann, and E. Calais (1998), Relative motions between the Caribbean and North American plates and related boundary zone deformation from a decade of GPS observations, *J. Geophys. Res.*, *103*, 15,157–15,182.

Duncan, R. A., and R. B. Hargraves (1984), Plate tectonic evolution of the Caribbean region in the mantle reference frame, in *The Caribbean-South American Plate Boundary and Regional Tectonics*, edited by W. Bonini, R. Hargraves, and R. Shagam, *Mem. Geol. Soc. Am.*, *162*, 81–93.

Duque-Caro, H. (1984), Structural style, diapirism and accretionary episodes of the Sinú-San Jacinto terrane, southwestern Caribbean boreland, in *The Caribbean-South American Plate Boundary and Regional Tectonics*, edited by W. Bonini, R. Hargraves, and R. Shagam, *Mem. Geol. Soc. Am.*, *162*, 303–316.

Duque-Caro, H. (1990), The Choco Block in the northwestern corner of South America: Structural, tectonostratigraphic, and paleogeographic implications, *J. S. Am. Earth Sci.*, *3*, 71–84.

Ego, F., M. Sébrier, A. Lavenu, H. Yepes, and A. Egues (1996), Quaternary state of stress in the northern Andes and the restraining bend model of the Ecuadorian Andes, *Tectonophysics*, *259*, 101–116.

Etayo-Serna, F., E. Parra, and G. Rodriguez (1982), Análisi facial del "Grupo del Dagua" con base en secciones aflorantes al oeste de Toro (Valle del Cauca), *Geol. Norandina*, *5*, 3–12.

Fabre, A. (1987), Tectonique et géneration d'hydrocarbures: Un modèle de l'evolution de la Cordillère Orientale de Colombie et du Bassin de Llanos pendant le Crétacé et le Tertiaire, *Arch. Sci.*, *40*, 145–190.

Freymueller, F. T., J. N. Kellogg, and V. Vega (1993), Plate motions in the north Andean region, *J. Geophys. Res.*, *98*, 21,853–21,863.

Gomez, E., and P. Pedraza (1994), El Maastrichtiano de la region Honda-Guaduas, límite del Valle Superior del Magdalena: Registro sedimentario de un delta dominado por ríos trenzados, in *Estudios Geológicos del Valle Superior del Magdalena*, vol. III, 20 pp., Univ. Nacl. de Colombia, Ecopetrol.

Gomez, E., T. Jordan, R. Almandiger, K. Hegarty, S. Kelly, and M. Heizler (2003), Controls on Architecture of the Late Cretaceous to Cenozoic southern Middle Magdalena Valley Basin, Colombia, *Geol. Soc. Am. Bull.*, *115*, 131–147.

Gutscher, M. A., W. Spakman, H. Bijwaard, and E. R. Engdahl (2000), Geodynamics of flat subduction: Seismicity and tomographic constraints from the Andean margin, *Tectonics*, *19*, 814–833.

Hey, R. (1977), Tectonic evolution of the Cocos-Nazca spreading center, *Geol. Soc. Am. Bull.*, *88*, 1404–1420.

Hu, J.-C., J. Angelier, J.-C. Lee, H.-T. Chu, and D. Byrne (1996), Kinematics of convergence, deformation and stress distribution in the Taiwan collision area: 2-D finite-element numerical modelling, *Tectonophysics*, *255*, 243–268.

Jullivert, M. (1970), Cover and basement tectonics in the Cordillera Oriental of Colombia, South America, and comparison with some other folded chains, *Geol. Soc. Am. Bull.*, *81*, 3623–3646.

Kammer, A. (1999), Observaciones acerca de un origen transpresivo de la Cordillera Oriental, *Rev. Geol. Colombiana*, *24*, 29–53.

Kellogg, J. N., and W. E. Bonini (1982), Subduction of the Caribbean plate and basement uplifts in the overriding South American plate, *Tectonics*, *1*, 251–276.

Kellogg, J., and V. Vega (1995), Tectonic development of Panama, Costa Rica and the Colombian Andes: Constraints from Global Positioning System geodetic studies and gravity, in *Geologic and Tectonic Development of the Caribbean plate Boundary in Southern Central America*, edited by P. Mann, *Spec. Pap. Geol. Soc. Am.*, *295*, 75–90.

Kroonemberg, S. (1982), A Grenvillian Granulite Belt in the Colombian Andes and its relations to the Guiana Shield, *Geol. Mijnbouw*, *61*, 325–333.

Laad, J. W. (1976), Relative motion of South America with respect to North America and Caribbean tectonics, *Geol. Soc. Am. Bull.*, *87*, 969–976.

Malave, G., and G. Suarez (1995), Intermediate-depth seismicity in northern Colombia and western Venezuela and its relationship to Caribbean plate subduction, *Tectonics*, *14*, 617–628.

Mann, P. (1999), Caribbean sedimentary basins: classification and tectonic setting from Jurassic to Present, in *Sedimentary Basins of the World*, vol. 4, *Caribbean Basins*, edited by P. Mann, pp. 3–31, Elsevier, New York.

Mauffret, A., and S. Leroy (1999), Neogene intraplate deformation of the Caribbean plate at the Beata Ridge, in *Sedimentary Basins of the World*, vol. 4, *Caribbean Basins*, edited by P. Mann, pp. 627–669, Elsevier, New York.

McCourt, W. J., J. A. Aspend, and M. Brook (1984), New geological and geochronological data from the Colombian Andes: Continental growth by multiple accretion, *J. Geol. Soc. London*, *141*, 831–845.

Meissnar, R. O., E. R. Flueh, F. Stibane, and E. Berg (1976), Dynamics of the active plate boundary in southwest Colombia according to recent geophysical measurements, *Tectonophysics*, *35*, 115–136.

Minster, J. B., and T. H. Jordan (1978), Present-day plate motions, *J. Geophys. Res.*, *83*, 5331–5354.

Mojica, J., and E. Scheidegger (1984), Fósiles deformados y otras estructuras microtectónicas en la Formación Hilo (Albiano): Alrededores de Sasaima, Cundinamarca, (Colombia), in *Rev. Geol. Colombiana*, *13*, 41–54.

Montes, C. (2001), Three dimensional structure and kinematics of the Piedras-Girardot fold-belt in the northern Andes of Colombia, Ph.D. thesis, 217 pp., Univ. of Knoxville, Tenn.

Montes, C., M. Baquero, D. Castillo, and M. Cortés (1994), Salt-related structures postdating thrust tectonics: An example from the Cordillera Oriental, Colombia, paper presented at Geological Society of America Annual Meeting, Seattle.

Müller, R. D., J. Y. Royer, S. C. Cande, W. R. Roest, and S. Maschenkov (1999), New constraints on the Late Cretaceous/Tertiary plate tectonics evolution of the Caribbean, in *Sedimentary Basins of the World*, vol. 4, *Caribbean Basins*, edited by P. Mann, pp. 33–59, Elsevier, New York.

Osorio, C., D. Michoux, and G. Tellez (2002), Stratigraphy of the Tertiary sequences-Upper Magdalena and Putumayo basins, a different point of view for hydrocarbon exploration, paper presented at II Convention of the Asociación Colombiana de Geólogos y Geofísicos del Petróleo, Bogotá.

Pennington, W. D. (1981), Subduction of the East Panama Basin and seismotectonics of the northwestern South America, *J. Geophys. Res.*, *86*, 10,753–10,770.

Pindell, J. L. (1985), Alleghenian reconstruction and subsequent evolution of the Gulf of Mexico, Bahamas, and Proto-Caribbean, *Tectonics*, *4*, 1–39.

Pindell, J. L., and S. F. Barret (1990), Geological evolution of the Caribbean region; A plate-tectonic perspective, in *The Geology of North America*, vol. H, *The Caribbean Region*, edited by G. Dengo, and J. E. Case, pp. 405–432, Geol. Soc. of Am., Boulder, Colo.

Pindell, J. L., and J. F. Dewey (1982), Permo-Triassic reconstruction of western Pangea and the evolution of the Gulf of Mexico/Caribbean region, *Tectonics*, *1*, 179–211.

Pindell, J. L., S. C. Cande, W. C. Pittman, D. B. Rowley, J. F. Dewey, J. Labreque, and W. Haxby (1988), A plate-kinematic framework for models of the Caribbean evolution, *Tectonophysics*, *155*, 121–138.

Pindell, J., L. R. Higgs, and J. F. Dewey (1998), Cenozoic palinpastic reconstruction, paleogeographic evolution and hydrocarbon setting of the northern margin of South America, in *Paleogeographic Evolution and Non-Glacial Eustacy, Northern South America*, *Spec. Publ. SEPM Soc. Sediment. Geol.*, *58*, 45–85.

Porta, J. D. (1965), La estratigrafía del Cretácico Superior y Terciario en el extremo S del Valle Medio del Magdalena, in *Bol. Geol. Univ. Ind. Santander*, *19*, 5–51.

Porta, J. D., and S. de Porta (1962), Discusión sobre la edad de las formaciones Hoyón, Gualanday y La Cira en la region de Honda-San Juan de Ríoseco (Valle del Magdalena), in *Bol. Geol. Univ. Ind. Santander*, *9*, 69–85.

Raasveldt, H. C. (1956), Mapa geológico de la República de Colombia, Plancha L-9 Girardot, scale 1:200,000, Minist. de Min. y Pet., Inst. Geol. Nacl., Bogotá.

Raasveldt, H. C., and J. M. Carvajal (1957), Mapa geológico de la República de Colombia, Plancha K-9 Armero, scale 1:200,000, Minist. de Min. y Pet., Inst. Geol. Nacl., Bogotá.

Restrepo-Pace, P. A. (1992), Petrotectonic characterization of the central Andean Terrane, Colombia, *J. S. Am. Earth Sci.*, *5*, 97–116.

Restrepo-Pace, P. A. (1995), Late Precambrian to early Mesozoic tectonic evolution of the Colombian Andes, Based on new geochronological, geochemical and isotopic data, Ph.D. thesis, 194 pp., Univ. of Ariz., Tucson.

Restrepo-Pace, P. A. (1999), Fold and thrust belt along the western flank of the Eastern Cordillera of Colombia: Style, kinematics and timing constrains derived from seismic data and detailed surface mapping, paper presented at Thrust Tectonic Conference, Royal Holloway, Univ. of London.

Restrepo-Pace, P. A., J. Ruiz, G. Gehrels, and M. Cosca (1997), Geochronology and Nd isotopic data of Grenvillian-age rocks in the Colombian Andes: New constraints for Late Proterozoic-early Paleozoic paleocontinental reconstructions of the Americas, *Earth Planet. Sci. Lett*, *150*, 427–441.

Ross, M. I., and C. R. Scotese (1988), A hierarchical tectonic model of the Gulf of Mexico and Caribbean region, *Tectonophysics*, *155*, 139–168.

Rowan, M., and R. Linares (2000), Fold Evolution matrices and axial-surface analysis of fault-bend folds: Application to the Medina Anticline, Eastern Cordillera, Colombia, *AAPG Bull.*, *84*, 741–764.

Ruiz, C., N. Davis, P. Bentham, A. Price, and D. Carvajal (2000), Structure and tectonics of the South Caribbean Basin, southern offshore Colombia: A progressive accretionary system, paper presented at VI Simposio Bolivariano Exploración Petrolera en las Cuencas Subandinas, Soc. Venez. de Geol., Caracas.

Sarmiento, L. F. (1989), Stratigraphy of the Cordillera Oriental west of Bogotá, Colombia, M.Sc. thesis, 102 pp., Univ. of S. C., Columbia.

Sarmiento, L. F. (2001), Mesozoic rifting and Cenozoic basin inversion history of the Eastern Cordillera, Colombian Andes, Ph.D. thesis, 295 pp., Vrije Univ., Amsterdam.

Suarez, M. A., M. P. Serrano, and M. Morales (2000), Estilos estructurales y potencial de entrampamiento de la sección Cretácea, cuenca del Valle Medio del Magdalena, paper presented at VII Simposio Bolivariano Exploración Petrolera en las Cuencas Subandinas, Soc. Venez. de Geol., Caracas.

Taboada, A., L. A. Rivera, A. Fuenzalida, A. Cisternas, H. Philip, A. Bijwaard, J. Olaya, and C. Rivera (2000), Geodynamics of the northern Andes: Subductions and intracontinental deformation (Colombia), *Tectonics*, *19*, 787–813.

Toto, E., and J. Kellogg (1992), Structure of the Sinu-San Jacinto fold-belt, an active accretionary prism in northern Colombia, *J. S. Am. Earth Sci.*, *5*, 211–222.

Trenkamp, R., J. N. Kellogg, J. T. Freymueller, and H. P. Mora (2002), Wide plate deformation, southern Central America and northwestern South America, CASA GPS observations, *J. S. Am. Earth Sci.*, *15*, 157–171.

Van der Hammen, T. (1958), Estratigrafía del Terciario y Maestrichtiano continentales y tectonogénesis de los Andes Colombianos, *Bol. Geol. Serv. Geol. Nacl.*, *5*, 67–128.

Van der Hilst, R. D., and P. Mann (1994), Tectonic implications of tomographic images of subducted lithosphere beneath northwestern South America, *Geol. Mijnbouw*, *22*, 451–454.

Villamil, T. (1999), Campanian-Miocene tectonostratigraphy, depocenter evolution and basin development of Colombia and western Venezuela, *Paleogeogr. Paleoclimatol. Paleoecol.*, *153*, 239–275.

Villamil, T., and J. L. Pindell (1998), Cenozoic Mesozoic paleogeographic evolution of the northern South America: Foundations for sequence stratigraphic studies in passive margin strata deposited during non-glacial times, in *Paleogeographic Evolution and Non-Glacial Eustacy, Northern South America*, *Spec. Publ. SEPM Soc. Sediment. Geol.*, *58*, 283–318.

Villamil, T., C. Arango, M. Suarez, C. Malagón, and R. Linares (1995), Discordancia Paleoceno-Eoceno y depósitos sobreyacentes en Colombia: Implicaciones tectónicas y de geología del Petróleo, paper presented at VI Congreso Colombiano del Petróleo, Asoc. Colombiana de Ing. de Pet., Bogotá.

Villarroel, C., and J. Mojica (1987), El Paleozoico Superior (Carbonifero-Permico) sedimentario de Colombia: Afloramientos conocidos y caracterísiticas generales, *Rev. Geol. Colombiana*, *16*, 81–87.

Ziegler, P. A., J.-D. Van Wess, and S. Cloetingh (1998), Mechanical controls on collision-related compressional intraplate deformation, *Tectonophysics*, *300*, 103–129.

J. Angelier, Laboratoire de Tectonique, Université Pierre et Marie Curie, Case 129, T56-E2, 4 Place Jussieu, F-75252 Paris Cedex 05, France.

B. Colletta, Institut Français du Pétrole, 1 et 4 Avenue de Bois-Préau Rueil-Malmaison, Cedex, F-92852, France.

M. Cortés, Corporación Geológica Ares, Bogotá, Colombia. (mcortes@cgares.org)